P517271.PDF [Page: 3 of 59]

Copy No. 8

DEFENCE R&D DÉFENSE

Constraint Effects on Fracture Toughness

G. Shen, S Xu & W.R. Tyson

Materials Technology Laboratory
Canada Centre for Minerals and Energy Technology (CANMET)
568 Booth Street,
Ottawa, Ontario
K1A 0G1

Defence R&D Canada

Contractor Report
DREA CR 2001-091
July 2001

National Defence Défense nationale

Canada

PS17271.PDF [Page: 4 of 59]

104-06988/

Copy No: _____

CONSTRAINT EFFECTS ON FRACTURE TOUGHNESS

G. Shen, S. Xu, & W.R. Tyson

Materials Technology Laboratory
Canada Centre for Minerals and Energy Technology (CANMET)
568 Booth Street,
Ottawa, Ontario
K1A 0G1

Defence Research Establishment Atlantic

Contractor Report

DREA CR 2001-091

July 2001

P517271 PDF [Page: 5 of 59]

Authors

G. Hen, X. Xu & W.R. Tyson

Approved by

W. Nethercote, Deputy Director General

for J. Morrison

Approved for release by

Kirk Foster

DRP Chair

The scientific or technical validity of this Contract Report is entirely the responsibility of the contractor and the contents do not necessarily have the approval or endorsement of Defence R&D Canada

© Her Majesty the Queen as represented by the Minister of National Defence, 2001

© Sa majesté la reine, représentée par le ministre de la Défense nationale, 2001

Abstract

Fracture resistance curves have been measured for a CSA 350WT ship plate using different a/W ratios, and stretch-zone-width (SZW) measurements have been made on the fracture surfaces. Associated calculations using finite element analysis (FEA) have also been performed, with special attention paid to the crack tip blunting behaviour

It has been confirmed that the fracture resistance increases with decreasing constraint, i e. with decreasing a/W It has also been shown that the blunting line slope $M\sigma_Y$ depends on constraint as well as on material properties. FEA results indicate that M lies between the value recommended in ASTM standards (M=2) and that suggested by the European Structural Integrity Society (ESIS) (M=4 for this material), being closer to the ESIS value

The subjective nature of the measurement made it difficult to derive reproducible SZW values, and a recently developed ESIS procedure produced very conservative results. It is difficult to clearly distinguish between the stretch zone and the tearing regions, particularly when the resistance curve data is described using a power-law equation This suggests that it would be preferable to define toughness by means of a value of J or CTOD at a specific amount of crack growth, e.g 0.2 mm, without distinguishing between blunting and tearing contributions.

Résumé

On a mesuré des courbes de résistance à la rupture d'une tôle navale CSA 350WT, en utilisant différents rapports de a/W. On a ensuite effectué des mesures de la largeur de la zone d'étirement (LZE) dans les sections de rupture. Les calculs connexes ont été effectués par analyse des éléments finis (AEF), en portant une attention particulière au phénomène d'émoussement en pointe de fissure.

Les résultats confirment que la résistance à la rupture augmente avec la diminution des contraintes, c'est-à-dire avec une valeur décroissante de a/W. Ils démontrent aussi que la pente de la droite d'émoussement $M\sigma_Y$ est fonction des contraintes, ainsi que des propriétés du matériau Les résultats d'AEF indiquent que la valeur M se situe entre celle recommandée dans les normes ASTM (M=2) et celle suggérée par l'European Structural Integrity Society (ESIS) (M=4, dans le cas du présent matériau), et qu'elle est plus proche de cette dernière.

La nature subjective des mesures effectuées ne facilite pas l'obtention de valeurs reproductibles de LZE et une méthode récemment élaborée par l'ESIS a produit des résultats très « prudents ». Il est difficile de bien distinguer la zone d'étirement et les sections de rupture, particulièrement lorsque les données des courbes de résistance sont définies en fonction d'une équation du type loi de puissance. Ces résultats semblent indiquer qu'il serait plus approprié de définir la ténacité à l'aide d'une valeur de J ou de CTOD, pour une valeur précise de la propagation de la fissure, par exemple à 0,2 mm, sans faire de distinction entre la contribution de l'émoussement et celle du déchirement.

P517271.PDF [Page: 7 of 59]

Executive summary

The crack growth resistance (toughness) of a structural material depends on the geometry of the crack and the type of loading. These produce differences in the crack tip stress state referred to as the "constraint". The stress state controls the deformation required to initiate fracture, and the mechanisms of fracture in steels are profoundly affected by the local constraint. Standardized techniques for toughness measurement in laboratory tests are conservatively designed to reflect a high degree of constraint, and thus provide a lower bound estimate of a material's resistance to fracture. They may thus yield results which are too conservative to be applied sensibly to a field situation, resulting in misleading conclusions during a failure analysis, or to onerous requirements for material selection.

To account for constraint effects, crack tip stresses must be defined not only by the conventional driving force used in standardized tests (i.e a stress intensity or an energy release rate), but also by a second parameter that can quantify crack tip constraint. This allows the constraint in the laboratory test to be matched to that of the crack found in service. This report describes the crack tip behaviour of a Canadian ship steel.

Morrison, J.. 2001. Contraint Effects on Fracture Toughness. DREA CR 2001-091
Defence Research Establishment Atlantic.

P517271.PDF [Page: 8 of 59]

Sommaire

Il existe une relation entre la résistance à la propagation de la fissure (la ténacité) d'un matériau structural, et la géométrie de la fissure et le type de charge. Ces deux éléments entraînent des différences au niveau de l'état de tension en pointe de fissure, lequel est désigné par le terme « contrainte ». L'état de tension contrôle la déformation nécessaire à l'amorce de la fracture et les mécanismes de fracture, dans les aciers, sont fonction, en grande partie, des contraintes localisées. La conception « prudente » des techniques normalisées qu'on utilise pour mesurer la ténacité en laboratoire leur permet de tenir compte de contraintes élevées et, de ce fait, elles fournissent une limite inférieure estimée de la résistance à la rupture du matériau. Par conséquent, elles peuvent produire des résultats qui sont trop « prudents » pour qu'on puisse les appliquer judicieusement à un cas de terrain, ce qui entraîne des conclusions erronées lors d'une analyse de défaillance, ou des exigences coûteuses en matière de sélection du matériau.

Afin de tenir compte des effets associés aux contraintes, la définition des tensions en pointe de fissure doit non seulement comprendre la force propulsive classique utilisée dans les essais normalisés (c'est-à-dire l'intensité de l'effort ou la vitesse de dégagement d'énergie), mais aussi un second paramètre qui permet de quantifier la contrainte en pointe de fissure. Cette solution permet de comparer la valeur de contrainte déterminée en laboratoire avec la valeur correspondante de la fissure observée dans le matériau en service. Le présent rapport contient la description du comportement en pointe de fissure d'un acier pour navires canadien.

Morrison, J., 2001. Contraint Effects on Fracture Toughness. DREA CR 2001-091
Defence Research Establishment Atlantic.

P517271.PDF [Page: 9 of 59]

TABLE OF CONTENTS

	Page
Abstract	i
Résumé	ii
Executive Summary	iii
Sommaire	iv
Table of Contents	v
List of Figures	vi
1.0 Introduction	1
2.0 Material and Finite Element Analysis (FEA)	2
3.0 J-Resistance Tests for SENB Samples at -30^{0}C	3
4.0 Crack Tip Blunting Analysis	7
5.0 Crack Tip Constraint Parameters	10
5.1 T-stress and parameter	11
5.2 Q parameter	12
6.0 Conclusions	15
7.0 Acknowledgments	16
References	16
Annexes	44

P517271.PDF [Page: 10 of 59]

List of figures

Figure 1. True Stress/true strain curve (A) and Ramberg-Osgood curve fits (B,C) 18

Figure 2. Normalized J-integral as a function of L_T 18

Figure 3. Specimen geometry (mm) 19

Figure 4a. J-resistance curve for Sample L2 20

Figure 4b. J-resistance curve for Sample L3 20

Figure 4c. J-resistance curve for Sample E5 21

Figure 4d. J-resistance curve for Sample E6 21

Figure 4e. J-resistance curve for Sample D1 22

Figure 4f. J-resistance curve for Sample D4 22

Figure 6a. Load vs. crack mouth opening displacement for Sample L2 23

Figure 6b. Load vs. crack mouth opening displacement for Sample L3 23

Figure 5c. Load vs. crack mouth opening displacement for Sample E3 24

Figure 5d. Load vs. crack mouth opening displacement for Sample E6 24

Figure 5e. Load vs. crack mouth opening displacement for Sample D1 25

Figure 5f. Load vs. crack mouth opening displacement for Sample D4 25

P517271.PDF [Page: 11 of 59]

Figure 6. J-resistance ($J_{0.2}$) as a function of a/W ($J_{0.2}$ is the J-resistance 26
at 0.2 mm crack extension measuremend directly by compliance unloading; the crack length was not revised by using ASTM E1820)

Figure 7. J-resistance curves for SENB samples (the initial crack lengths 26
have been revised by suing eqn (A11.1) in ASTM E1820)

Figure 8. d_n as a function of normalized J-integral, calculated for actural σ ε data 27

Figure 9. Blunting line for SENB geometry (a/W=0.5); 27

Figure 10. Finite element mesh for a SENB sample and its deformed crack tip 28

Figure 11. $J_{0.2}$ vs β_T for SENB samples with different a/W 29

Figure 12. Finite element mesh for boundary layer method 29

Figure 13. Normalized opening stress at crack tip under plan strain small-scale 30
yielding (SYY)

Figure 14. Normalized crack opening stress as a function of 31
normalized distance from crack tip, a/W=0.2

Figure 15. Normalized crack opening stress as a function of 31
normalized distance from crack tip, a/W=0.5

Figure 16. Q as a function of applied driving force for SENB geometry 32

Figure 17. $J_{0.2}$ as a function of β_Q for SENB samples 32

1.0 - INTRODUCTION

It been known for some time that the resistance to crack growth (toughness) of a structural material may vary depending on the geometry of the crack and the mode of loading. This is a result of the varying degree of triaxiality of the stresses at the crack tip, which is referred to as the "constraint". For example, the plastic zone of a deep crack in a thick material is surrounded entirely by elastic material and is therefore highly constrained, while the plastic zone of a shallow crack may spread back to the free surface and can thereby relieve the level of triaxial stress. Triaxiality, broadly defined as the ratio of hydrostatic stress to shear stress, controls the level of tensile stress in the plastic zone and thereby strongly affects the extent of deformation required to initiate fracture in the plastic zone. Both of the major micromechanisms, cleavage (brittle) and microvoid coalescence (ductile), are affected by triaxiality.

The practical result of this is that the toughness measured in a laboratory test, which is conservatively designed to have a high degree of triaxiality, may be greatly conservative when applied to a field situation. This may lead to misleading conclusions in a failure analysis, or to excessively onerous requirements for material selection.

It has become possible recently to account for constraint effects in a quantitative way, using "two-parameter fracture mechanics". In this approach, the crack tip stresses are defined not only by the conventional driving force, K or J, but also by a second parameter, T or Q, that describes the degree of triaxiality. This allows the toughness to be measured as a function of the constraint, and thereby to match the constraint of the laboratory test to be matched to the constraint of the crack in service.

The fracture toughness of a ship steel plate of grade CSA G40.21 350WT has been characterized over a range of constraint conditions by testing three-point bend bars pre-cracked to different crack depths. The tests were performed at room temperature where the mode of fracture was ductile tearing (microvoid coalescence), and resistance curves (J-integral as a function of crack growth) were calculated. The results for initiation toughness (J at 0.2 mm crack growth) and growth resistance (tearing modulus, or shape of the resistance curve) have been characterized in both the linear-elastic K/T and elastic-plastic J/Q formats.

In addition, FEM has been used to determine numerically the crack-tip stress fields (opening stress versus distance from crack tip) at each a/W for a series of increasing J values (a series of values of J/(ligament x yield stress). Q has been evaluated as a function of J. The size effect has also been studied to determine the minimum ligament length at which the two-parameter description becomes invalid. This indicates the point at which the stress fields are no longer controlled by J and Q within a "significant" distance of the crack tip.

P517271 PDF [Page: 13 of 59]

2.0 - MATERIAL AND FINITE ELEMENT ANALYSIS

The material used in the present study was a 15 mm CSA grade G40.21 350WT plate. The tensile properties of the steel at –30°C measured at the DREA Dockyard Laboratory Pacific (DLP) are listed in Table 1.

Table 1 Tensile properties of CSA G40.21 350WT at –30°C

Elongation (%)	0.2 % Yield Strength (MPa)	Ultimate Strength (MPa)
44.1	508	631

Fig. 1 shows the measured true stress/true strain properties of the steel at –30°C (points A) and also two fitted curves (B and C) described by the following Ramberg-Osgood equation:

$$\frac{\varepsilon}{\varepsilon_0} = \frac{\sigma}{\sigma_0} + \alpha\left(\frac{\sigma}{\sigma_0}\right)^n \qquad (1)$$

Curves B and C were created by fitting the data from the measured true stress/true strain curve optimizing the fits to the yield and post-yield behaviour respectively. Curve B provides a good fit to the initial yield stress but a poor fit to the plastic part of the actual true stress/true strain curve. Curve C, on the other hand, provides a good fit to the post-yield (plastic) behavior, but a poor fit in the yield region of the actual true stress/true strain curve. The fitted coefficients n and α are listed in Table 2, where the 0.2% yield strengths were used as σ_0 and in the calculation of $\varepsilon_0=\sigma_0/E$ (with E=207 GPa). Evidently, the R-O equation (1) does not fit the actual data well over the whole range, which is expected in cases where there is a significant yield plateau.

Table 2 Ramberg-Osgood parameters

Curves	n	α	σ_0 (MPa)	ε_0
B	11.0	0.95	508	0.00245
C	5.2	8.84	508	0.00245

These three relations (actual stress-strain data A, and R-O curve fits B and C) were used to study the effect of material properties on crack driving force. Two-dimensional plane strain finite element analysis was conducted on a standard single edge notch three-point-bend (SENB) specimen (a/W=0.5, W=30 mm), with the curves being employed in three different calculations. Owing to the symmetry, only half of the sample was modeled. The mid-span load applied to the SENB samples was distributed over two small element surfaces (each 1 mm in length) to minimize effects of the local singularity of an idealized point load. In the modeling, eight-node isoparametric displacement-based elements were used. At the crack tip, the elements were collapsed to allow stress singularity at the crack front. In the elastic-plastic regime, conventional small strain theory was used. The finite element code used in the study was ADINA. The applied load was gradually increased from 0.2 to 1.4 times the limit load defined below in 30 to 50 steps. The Virtual Crack Extension (VCE) method was used to calculate the J-integral.

Fig. 2 shows the normalized J-integral ($J/(a\sigma_0)$) as a function of the normalized load L_r ($L_r=P/P_0$) where a is the crack length and σ_0 is the yield strength, P is the load per unit thickness and P_0 is the limit load per unit thickness. P_0 is defined as the plastic collapse load for perfectly plastic material corresponding to n=4. Following the preferences of the EPRI handbook [1], for plane strain, the Green and Hundy solution [2] was used, giving $P_0=0.782\sigma_0c^2/L$ (where c is the remaining ligament length and L is the half span of the SENB sample). It is seen in Fig. 2 that the crack driving force of the actual material can be approximated with reasonable accuracy by that of Curve B within the range $0\leq L_r \leq 1.0$, and by that of Curve C when $L_r\geq 1.2$. The actual true stress/true strain curve was used as input for the FEA calculations reported below.

3.0 - J-RESISTANCE TESTS USING SENB SAMPLES AT –30°C

Fig. 3 shows the geometry of the 20% side-grooved B×2B SENB samples tested in this study. For all samples W=30 mm, B=15 mm, and B_n=12 mm. The specimens were machined and fatigue precracked at DLP. There were three pairs of samples, with initial a/W values of nominally 0.2, 0.5, and 0.7. Tests were done in three-point bending in an Instron universal testing machine, at a test temperature of -30°C. To ensure a stable and uniform test temperature, the cold chamber temperature was controlled at -30°C for about two hours before starting the test. For each test, two thermocouples, one attached to the test sample and the other to the upper roller (opposite the notch), were used to measure the temperature. Readings from the two thermocouples agreed to within ± 1°C. After reaching the test temperature, samples were soaked for at least 20 min., and the temperature was also maintained at –30 ± 1°C during loading, which usually lasted about an hour. After testing, the samples were heat tinted and then broken open in liquid nitrogen. The initial and final crack lengths were then measured using the 9-point technique described in ASTM E1820 [3], and are reported in Table 3.

Table 3 Crack lengths of SENB samples

Specimen ID	a_0/W	a_f/W
L2	0.193	0.239
L3	0.195	0.247
E5	0.494	0.519
E6	0.495	0.549
D1	0.709	0.777
D4	0.711	0.774

There are requirements in ASTM Standard E1820 on crack front straightness, stated in terms of the maximum allowable difference between the measured crack lengths, and the uniformity of crack extension. Values of the maximum difference between the nine physical measurements of initial and final crack lengths and the crack extensions, expressed as a percentage of the respective average values, are reported in Table 4. The maximum differences allowed by ASTM E1820 are also listed in the table for comparison. It is seen that the allowable maximum differences have been exceeded in some cases, and these are underlined in the table. In these cases, significant splitting was observed on the fracture surfaces. Also, values of a/W were used in the present study which are outside the range covered in ASTM E 1820, which requires the initial crack length to be between 0.45 and 0.70W. Consequently, no allowable maximum differences in 9-point measurements have been defined in the ASTM standard for shallow cracks.

Table 4 Maximum deviation of crack lengths from average values

Specimen ID	Initial a_0 (%)	Final a_f (%)	Crack extension (%)
L2	5.7	3.3	15.5
L3	4.9	10.4	31.3
E5	2.1	3.3	51.8
E6	2.3	5.8	70.1
D1	1.5	2.5	30.8
D4	2.1	0.6	23.3
ASTM E 1820	≤5	≤5	≤50

Crack lengths were measured during testing using the unloading compliance technique. The results are compared with physically measured (9-point) crack lengths in Table 5. The CMOD unloading compliance expression in ASTM E 1820 was used to estimate crack length; this expression is valid for all of the a/W values. It is seen that the difference of crack lengths measured by these two methods is of the order of 5% for shallow cracks (a/W≈0.2) and 1% for deep cracks (a/W≈0.7).

Table 5. Crack length measured by 9-point and by compliance unloading techniques

Specimen I.D.	a_0 (mm)			a_f (mm)		
	9-point	Compliance	Difference (%)	9-point	Compliance	Difference (%)
L2	5.78	5.75	0.52	7.16	7.47	4.33
L3	5.85	5.64	3.59	7.41	7.81	5.40
E5	14.82	15.2	2.56	15.56	15.71	0.96
E6	14.86	15.05	1.28	16.46	16.67	1.28
D1	21.27	21.32	0.24	23.3	22.9	1.72
D4	21.32	21.24	0.38	23.23	22.99	1.03

J-resistance curves were measured following the procedures of ASTM E1820 with some modification of the J-integral evaluation for application to shallow cracks. For the present purpose of studying the effect of constraint, the criteria used in ASTM E1820 for maximum J-integral capacity were ignored. These require that J_{max} be the smaller of:

$$J_{max} = \frac{b\sigma_y}{20} \tag{2}$$

and

$$J_{max} = \frac{B\sigma_y}{20} \tag{3}$$

The effects of constraint are characterized using the T-stress or Q parameter described in Section 5. The plastic part of the J-integral was calculated using the equation given in ASTM E1820:

$$J_{pl(i)} = \left[J_{pl(i-1)} + \left(\frac{\eta}{b_{(i-1)}} \right) \left(\frac{A_{pl(i)} - A_{pl(i-1)}}{B_N} \right) \right] \left[\gamma - \frac{a_{(i)} - a_{(i-1)}}{b_{(i-1)}} \right] \quad (4)$$

where J_{pl}, A_{pl}, a, and b are plastic J, area under load/plastic load line displacement curve, crack depth, and ligament length respectively, and subscripts i and i-1 designate measurement points along the deformation curve. B_N is the net thickness. For deep cracks ($a/W \geq 0.5$), values of $\eta=2$ and $\gamma=1$ have been used following ASTM E1820. For shallow cracks, η and γ are functions of crack depth. In the present study, the values of η and γ given by Joyce et al. [4] were used: $\eta=2$ and $\gamma=1$ for $a/W \geq 0.282$, and for $a/W < 0.282$:

$$\eta = 0.32 + 12\left(a/W\right) - 49.5\left(a/W\right)^2 + 99.8\left(a/W\right)^3 \quad (5)$$

and

$$\gamma = \frac{\sum_{i=0}^{6} M_i \left(a/W\right)}{\sum_{i=0}^{3} N_i \left(a/W\right)} \quad (6)$$

The constants M_i and N_i given by Joyce et al. [4] are listed in Table 6.

Table 6 Constants M_i and N_i ([4], corrected*)

M_0	M_1	M_2	M_3	M_4	M_5	M_6
-12.22	106.7	-236.58	-924.6	4845.45	9880	9960
N_0	N_1	N_2	N_3			
0.32	12	-49.5	99.8			

* some printing mistakes appearing in reference [4] have been corrected.

The measured J-resistance curves are shown in Figs. 4a to 4f. The corresponding load/crack mouth opening displacement (CMOD) curves are shown in Figs. 5a to 5f. Values of J at $\Delta a=0.2$ mm (defined in the present study as $J_{0.2}$, which is the J-resistance at 0.2 mm crack extension measured directly by compliance unloading; the crack length was not revised by using ASTM E1820) are shown in Fig. 6 as a function of the initial value of a/W.

4.0 - CRACK TIP BLUNTING ANALYSIS

The measured J-resistance curves are shown in Fig. 7. (the initial crack lengths have been revised by using eqn (A11.1) in ASTM E1820). Also shown in Fig. 7 are three different blunting lines, which can be described by the following equation:

$$J = M\sigma_y \Delta a \qquad (7)$$

M is a constant and $\sigma_y=0.5(\sigma_{YS}+\sigma_{TS})$, where σ_{YS} and σ_{TS} are yield strength and ultimate strength respectively. Two of the lines correspond to the M values recommended by ASTM in E1820 [3] and by the European Structural Integrity Society (ESIS) in P2-92 [5], which are M=2 and M=4 respectively. The blunting line recommended by ESIS is actually dependent on yield stress and work hardening coefficient, and is given approximately in [5] by $M=3.75\sigma_{TS}$; for the material in this study, M is close to 4. The third blunting line (FEA) was determined by finite element calculation in the course of the present work as described in detail below, by monitoring the shape of the crack tip as well as calculating the J-integral as the load was increased. This FEA blunting line lies close to the ESIS line. The initial slope of the experimental data is also best described by the FEA or ESIS lines, although for small amounts of crack growth the data is complicated by the apparent "negative growth", particularly for the shallow crack (a/W≈0.2). This phenomenon has been observed previously, and reflects experimental difficulties with the compliance technique for shallow cracks. However, for the results obtained using the deep-crack samples (a/W≈0.7), "negative growth" is negligible and the data clearly follows the FEA/ESIS lines. Note that both the ASTM and ESIS blunting lines are for plane strain, and do not include constraint corrections for shallow cracks. The FEA line shown also refers to a highly constrained geometry, a/W=0.5. The effects of constraint on the blunting line are discussed below.

The blunting line was obtained from FEA as follows. The crack tip opening displacement (CTOD, or δ_t) is commonly defined as the distance between the intersections of the crack surfaces with the two sides of a right angle at the crack tip. According to this definition, $\delta_t=2\Delta a$. The CTOD is related to the J-integral through a parameter d_n which is a function of material properties and geometry. As written by EPRI [1],

$$\delta_t = d_n(\alpha\varepsilon_0, n)\frac{J}{\sigma_0} \qquad (8)$$

where σ_0 is yield strength and $\varepsilon_0 = \sigma_0 / E$. Combining this equation with eqn. (7), also assuming (approximately) that $\sigma_y=1.15\sigma_0$ and noting that $\delta_t=2\Delta a$, we have:

$$J = \frac{2\sigma_0 \Delta a}{d_n(\alpha\varepsilon_0, n)} = M\sigma_y \Delta a \qquad (9)$$

where $M=2/(1.15d_n(\alpha\varepsilon_0, n))$. For a plane strain SENB sample with a/W=0.5 and a material with n=10 and ε_0=0.00245, EPRI reports that $d_n(\alpha\varepsilon_0, n)$=0.55 [1], which results in M=3.16. Fig. 8 shows the d_n values for a SENB sample (a/W=0.5) calculated in the present study using the measured true stress/true strain curve as material input to a two-dimensional plane strain finite element calculation. The J-integral results for this material are best approximated (Fig. 2) using Ramberg-Osgood fit B with n=11 and ε_0=0.00245 for loads below the limit load. It is seen (Fig. 8) that d_n is approximately constant (≈0.54) over a wide range of J-integral values. The value of d_n calculated in the present study is close to the 0.55 given by EPRI for similar R-O parameters [1]. Fig. 9 shows the corresponding blunting line for the present results using the actual stress-strain curve. The slope of calculated blunting line is 1881 (kJ/m^2)/(mm) which gives a value of M=3.30. The blunting line recommended by ASTM E 1820 (M=2) and by ESIS (M=4) are also shown in Fig. 9 for comparison. These three blunting lines have previously been shown in Fig. 7.

Fig. 10 shows the finite element mesh used in the present calculations for a SENB sample (a/W=0.5) and the shape of the deformed crack tip. Note that d_n is a function of crack tip constraint, for example of a/W (in-plane) or the extent of plane strain or plane stress (through thickness). This has been recognized in the EPRI handbook [1] in which separate figures of d_n as a function of 1/n are shown for plane stress and plane strain. Note, however, that the captions in Figs 3-1 and 3-2 of [1] should be interchanged.

O'Dowd and Shih [6] proposed that d_n in eqn. (8) should be written as a function of the constraint parameter Q as well as material properties:

$$\delta_t = d_n(\alpha\varepsilon_0, n, Q)\frac{J}{\sigma_0} \qquad (10)$$

The significance of the Q parameter will be discussed in a following section. According to eqn. (10), the slope of a blunting line is a function of Q; with, in general, d_n increasing as Q decreases. Since the value of Q is smaller (i.e. constraint is lower) for a shallow crack than for a deep one, the blunting line for a shallow crack should fall below that of a deep crack. The results of FEA in the present study confirm this behaviour. Table 8 shows the parameter M in the equation for the blunting line (eqn. 7) for different material properties (σ_0, n) and crack depths (a/W) calculated by FEA in the present study using the Ramberg-Osgood constitutive equation. It is seen that the values of M decrease with decreasing a/W for constant material properties. Also, M decreases with increasing n for constant a/W, indicating that constraint loss occurs more readily when work hardening is low (i.e. when n is large).

For a/W=0.5, the average value of M in Table 7 for n values of 7, 13, and 20 is 3.5, very close to the FEM results for the present work using the experimental stress-strain data and much closer to the ESIS recommendation than that of ASTM. A representative value of M=3.3 has been used in the present work in calculating J values from stretch-zone-width measurements.

Table 7 Parameter M as a function of n and a/W

σ_0(MPa)	n	a/W	M
528	4.5	0.1	3.64
528	4.5	0.6	4.17
508	7	0.2	3.63
508	7	0.5	4.13
508	13	0.2	2.90
508	13	0.5	3.32
508	20	0.2	2.72
508	20	0.5	3.07

The initial slope of the experimental resistance curves agrees well with the FEM calculations, and there is a noticeable decrease in slope as crack growth proceeds. This behaviour is often approximated by a power-law relation of J with Δa, with an exponent typically ranging between 0.3 and 0.7. An example is shown in Fig. A5 labelled "power law regression line". Initiation of ductile tearing follows crack-tip blunting, with the amount of blunting dependent on the toughness of the material. It is often considered that there is a clearly defined demarcation between blunting and tearing, although in reality the initiation of tearing is difficult to define and measure unambiguously. Attempts have been made to devise a systematic procedure based on the observation of stretch-zone width (SZW) to measure the extent of blunting, i.e. of the crack growth due to blunting, at which initiation occurs. However, from a practical point of view, the resistance to ductile tearing is well described by the parameters of the power law describing the resistance curve. The magnitude of J at a fixed amount of total crack growth near initiation, e.g. 0.2 mm, is a useful toughness value and has been reported in Fig. 6. However, the mechanism of crack extension for large amounts of crack growth, i.e. by blunting or by ductile tearing, is also of interest. The present calculations indicate that continued blunting would correspond to a proportional increase of J and Δa as shown in Fig. 9, and so a significant deviation from linearity implies the onset of ductile tearing.

The fact that the early part of the resistance curve can normally be adequately described by a power-law fit implies that the onset of tearing is a gradual process that begins virtually from the start of loading.

To confirm that ductile tearing was in fact occurring in the present material for crack extensions even below a few tenths of a mm as implied by the results shown in Fig. 7, fractographic analysis was performed using the scanning electron microscope (SEM). Ductile tearing was in fact observed, and the detailed fractography and measurement of the stretch zones are described in Appendix A. Stretch zone widths were measured on three samples, L2, E6 and D1, with a/W approximately 0.2, 0.5 and 0.7 respectively. It was found that the width of the stretch zone measured according to a procedure recommended by ESIS (see [A3]) was less than 0.03 mm for all the samples examined. This is a surprisingly small value. The definition used in the measurement of SZW gave quite conservative values, and using the more common procedure of estimating the position of the crack front at tearing initiation by "best judgment" it was found that somewhat larger values (average SZW of 0.076 mm) result. However, the procedure is quite subjective and differences of typically 25% are found when the SZW is measured on the same fractographs by different researchers. However, it is clear that ductile tearing initiated within a tenth of a mm of crack extension by blunting.

5.0 - CRACK TIP CONSTRAINT PARAMETERS

The load and J-resistance at Δa=0.2 mm (defined as $J_{0.2}$ in the present study which is the J-resistance at 0.2 mm crack extension measured directly by compliance unloading; the crack length was not revised by using ASTM E1820) and at maximum load are reported in Table 8, and $J_{0.2}$ is shown as a function of a/W in Fig. 6. It can be seen that the shallow cracks have significantly higher J-resistance than the deep cracks.

Table 8 Load and J-resistance

Specimen I.D.	Pat Δa=0.2 mm (kN)	J_{02}(kJ/m^2)	Pmax (kN)	J at Pmax (kJ/m^2)
L2	48.48	416.5	>54.16	>1292.5
L3	48.93	453.8	54.19	1392.9
E5	20.48	312.9	>20.86	>575.2
E6	20.49	315.9	21.53	680.9
D1	7.64	268.9	7.74	369.1
D4	7.56	318.4	7.74	471.9

It is well known that the major micromechanisms of fracture, both cleavage and microvoid coalescence, are affected by triaxiality of the stresses at the crack tip. The degree of triaxiality of stress, referred to as the "constraint", is a function of the geometry of the crack and the mode of loading. In the elastic-plastic regime, it is also a function of the load.

$$\sigma_{ij} = \sigma_0 f_{ij}\left[r/(J/\sigma_0), \theta; (T/\sigma_0) \text{ or } Q\right] \tag{11}$$

Quantitative characterization of crack-tip states by the use of a second parameter in addition to K or J leads to a so-called "two-parameter fracture mechanics" in which the stresses at a crack tip are controlled by either T [7, 8] or Q [6, 9] as well as K or J.

5.1. T-stress and parameter β

In the elastic regime, the T-stress and a T-stress related parameter β have been used to characterize the triaxiality of crack tip stress fields [7, 8]. The T-stress is a stress parallel to the crack flanks that is found in the non-singular part of the elastic crack-tip solution as follows [7]:

$$\begin{bmatrix} \sigma_{11} & \sigma_{12} \\ \sigma_{21} & \sigma_{22} \end{bmatrix} = \frac{K}{\sqrt{2\pi r}} \begin{bmatrix} f_{11}(\varphi) & f_{12}(\varphi) \\ f_{21}(\varphi) & f_{22}(\varphi) \end{bmatrix} + \begin{bmatrix} T & 0 \\ 0 & 0 \end{bmatrix} \tag{12}$$

The "biaxiality parameter" β is defined as [7]:

$$\beta = T\sqrt{\pi a}/K \tag{13}$$

Values of β calculated by a variety of researchers for the SENB geometry have been reviewed in a previous study [10] and the most reliable solutions fitted by the following polynomial equations:

$$\beta = -0.46 + 0.236(a/W) + 6.410(a/W)^2 - 12.638(a/W)^3 + 8.422(a/W)^4 \tag{14}$$

The fracture resistance for samples with different constraint was also correlated using the normalized T-stress, β_T, defined by Ainsworth [11] as:

$$\beta_T = \frac{T}{\sigma_{ys} L_r} \tag{15}$$

Fig. 11 shows $J_{0.2}$ as a function of the normalized T-stress β_T. It is seen that the J-resistance decreases as the constraint parameter β_T increases.

5.2. Q parameter

In the elastic-plastic regime, a parameter termed Q has been proposed to characterize the triaxiality of crack tip stress fields [6, 9], defined as [9]

$$Q = \frac{\sigma_{\theta\theta} - (\sigma_{\theta\theta})_{HRR}}{\sigma_0} \tag{16}$$

where the opening mode stress $\sigma_{\theta\theta}$ is evaluated at $\theta=0$ and $r=2J/\sigma_0$. θ, J and σ_0 are angular coordinate at the crack tip, J-integral and yield strength respectively. $(\sigma_{\theta\theta})_{HRR}$ is the asymptotic (Hutchinson-Rice-Rosengren) solution for the crack-tip stress field. An alternative definition has been proposed by Dodds et al. [12] in which $(\sigma_{22})_{SSY}$ is used instead of $(\sigma_{22})_{HRR}$ in eqn. (16), i.e.

$$Q = \frac{\sigma_{\theta\theta} - (\sigma_{\theta\theta})_{SSY}}{\sigma_0} \tag{17}$$

where $(\sigma_{22})_{SSY}$ is the small-scale-yielding stress ahead of the crack calculated from a small-strain-theory boundary layer analysis [12]. Because $(\sigma_{22})_{SSY}$ is smaller than $(\sigma_{22})_{HRR}$ for the same material at the same loading condition (8% lower for n=10 at $r=2J/\sigma_0$, according to the calculation by Dodds et al. [12]), a larger value of Q is usually obtained from eqn. (17) than that from eqn. (16). Therefore, it is necessary to systematically apply

either eqn. (16) or eqn. (17) in the same study. Values of $(\sigma_{22})_{HRR}$ for different strain hardening exponents can be found from Shih's numerical solution [13] for Ramberg-Osgood materials with different n values. However, because the material used in the present study is not well described by a Ramberg-Osgood equation the Shih results are not suitable, and so the Dodds definition of Q, eqn. (17), has been used in the present work. A finite element program has been developed to calculate $(\sigma_{22})_{SSY}$ by boundary layer analysis. In the program, the displacements of the elastic singular field for mode I on an outer circular boundary were imposed using the following equations [12]:

$$\Delta u(r,\theta) = \frac{(1+\nu)\Delta K_I}{E}\left(\frac{r}{2\pi}\right)^{1/2}(3-4\nu-\cos\theta)\cos\left(\theta/2\right) \qquad (18)$$

and

$$\Delta v(r,\theta) = \frac{(1+\nu)\Delta K_I}{E}\left(\frac{r}{2\pi}\right)^{1/2}(3-4\nu-\cos\theta)\sin\left(\theta/2\right) \qquad (19)$$

Fig. 12 shows the finite element mesh and the applied displacements on the circular boundary. To ensure accurate description of small-scale yielding displacements at the boundary, 60 angular segments (fans) instead of the 18 which were suggested in [12] were used in the present study. Values of applied stress intensity factor (K_I^{appl}) at loading step i was obtained by summing ΔK from step 1 to i. The path-independent J-integral was then calculated by the virtual crack extension method. Values of the calculated stress intensity factor (K_I^{cal}) at loading step i were then deduced from the J-integral ($K_I^{cal}=(JE')^{1/2}$). To keep a small-scale yielding (SSY) stress condition, the applied stress intensity factors were kept small to ensure that the stress intensity factors calculated from the J-integral ($K_I^{cal}=JE/(1-\nu^2)$) were only slightly smaller than the applied stress intensity factors (K_I^{appl}) on the boundary (K_I^{appl} is applied in the boundary conditions of displacements); in the present study, $K_I^{cal}/K_I^{appl} \geq 0.95$. Fig. 13 shows the calculated normalized crack tip opening stress σ_{22}/σ_0 at the limit of small scale yielding, K_I^{cal}/K_I^{appl} .0.95, by using the boundary layer method. From the curve, it is seen that the normalized opening stress (σ_{op}/σ_0) is 3.00 at the $r=2J/\sigma_0$

Finite element analysis was also conducted for SENB samples with different a/W. Fig. 14 shows the calculated normalized crack tip opening stress σ_{22}/σ_0 for a shallow crack, a/W=0.2 at different crack driving force levels $J/(b\sigma_0)$. The crack opening stress for SSY is also shown in the figure for comparison. It can be seen that the crack opening stress for this

shallow-crack geometry is much lower than that of SSY at the same normalized distance $x/(J/\sigma_0)$ from crack tip. Also, the difference increases with increase of the crack driving force level $J/(b\sigma_0)$. Fig. 15 shows the calculated normalized crack tip opening stress σ_{22}/σ_0 for a deep crack, a/W=0.5, at different crack driving force levels $J/(b\sigma_0)$. Again, the crack opening stress for SSY is shown for comparison. It is seen that the crack opening stress at $x/(J/\sigma_0)=2$ for the deep-crack geometry is close to that of SSY at sufficiently small crack driving force levels ($J/(b\sigma_0)\leq 0.012$). However, it is lower than that of SYY when the crack driving force level increases. By comparing Figs. 14 and 15, it is seen that the calculated normalized crack opening stress σ_{22}/σ_0 is much lower in the shallow-crack than in the deep-crack geometry at the same normalized distance $x/(J/\sigma_0)$ from the crack tip at the same normalized crack driving force. This is doubtless a reason why the J-resistance for the shallow cracks is higher than for deep cracks.

Fig. 16 shows the calculated Q parameter as a function of normalized driving force $J/(b\sigma_0)$ for a/W=0.2, 0.3, 0.5 and 0.7. It is seen that Q decreases with increasing normalized crack driving force $J/(b\sigma_0)$. It also decreases with decreasing a/W. Fig.17 shows the measured crack resistance $J_{0.2}$ for SENB samples with both shallow and deep cracks as a function of constraint parameter β_Q with β_Q defined by Ainsworth [11] as:

$$\beta_Q = \frac{Q}{L_r} \tag{20}$$

The constraint parameter β_Q is a function of geometry, material strain hardening properties and load. It is seen that the fracture resistance of a cracked sample decreases with increasing β_Q. Table 9 lists the applied load L_r and the value of constraint parameters β_T and β_Q at Δa=0.2mm for all the samples tested.

Table 9 Applied load and constraint parameters

Sample I. D.	L_r	β_Q	β_T
L2	1.137	-0.732	-0.338
L3	1.153	-0.744	-0.332
E5	1.234	-0.400	0.161
E6	1.239	-0.402	0.161
D1	1.420	-0.341	0.283
D4	1.425	-0.431	0.284

P517271.PDF [Page: 26 of 59]

6.0 - CONCLUSIONS

The following conclusions can be drawn from the experiments and finite element analyses:

1) For driving force calculation, the stress/ strain curve of steel CSA G40.21 350WT could be modeled with reasonable accuracy by one Ramberg-Osgood curve (n=11, α=0.95) when the applied load is small ($L_r \leq 1$) and by another Ramberg-Osgood curve (n=5.2, α=8.84) when the applied load is large ($L_r \geq 1.2$). However, it could not be modeled for the whole loading range by using a single Ramberg-Osgood fit.

2) At –30°C the CSA G40.21 350WT steel fractured in a ductile fashion. For both deep and shallow notched samples, crack initiation occurred by ductile tearing from the stretch zone. From fractographic observations, the stretch zone width was observed to range from 0.02 to 0.10 mm, with the results being sensitive to how the "stretch zone" was defined and to subjective judgment. Using a conservative definition, values ranged from 0.017 to 0.022 mm, and using the best judgment of three observers, values ranged from 0.061 to 0.104 mm.

3) J-resistance curves for shallow cracks can be measured by using ASTM E1820 with modification of the parameters in the equation for calculating the J-integral to make it applicable to lower a/W values. The crack-length-dependent parameters η and γ given by Joyce et al. were used for shallow cracks in the present work.

4) Blunting line analysis was conducted by calculating the J-integral and crack tip opening displacement using the finite element method. The results from calculations conducted in the present study agreed with those given by EPRI. The slope of the blunting line for a deep crack (a/W=0.5) and a medium-hardening material (n=10, ε_0=0.00245) was found to correspond to $M = J/(\sigma_Y a) \cong 3.3$, which lies between values recommended by ASTM E 1820 (M=2) and by ESIS (M=4 for the present material).

5) The slope of the blunting line $M\sigma_Y$ is a function of material properties (yield stress and strain hardening coefficient) and of the crack tip constraint. M decreases with increasing strain hardening coefficient n at constant a/W, and increases with increasing a/W at constant n.

6) The crack tip stress field of a shallow crack is significantly lower than that of small scale yielding under the same applied driving force. The difference increases with increasing applied stress. The crack tip stress field of a deep crack is close to that of small scale yielding under the same applied driving force when the applied crack driving force is small. However, it is lower than that of SSY when the applied load is large.

7) Shallow cracks have much higher J-resistance than deep cracks. The J-resistance of SENB samples with different crack depth was well correlated by either β_T, related to the T-stress, or by β_Q , related to the Q parameter.

8) The SZW was found to be very small (less than 0.1 mm). However, no dependence of SZW on initial crack length was found. In particular, the SZW was not found to be larger at a/W=0.2 than at a/W=0.5 or 0.7.

7.0 - ACKNOWLEDGMENTS

The authors are grateful to Mr. Real Bouchard for developing software for the J-resistance tests, and Ms. R. Zavadil for performing optical macrography.

8.8 - REFERENCES

[1] Kumar, V. German, M. D. and Shih, C. F., An Engineering Approach for Elastic-Plastic Fracture Analysis, NP-1931, Research Project 1237-1, 1981

[2] Green, A. P. and Hundy, B. B., Initial Plastic Yielding in Notch Bend Bars, *Journal of the Mechanics and Physics of Solids*, vol. 4, pp. 128-144, 1956

[3] ASTM E 1820 (1996), Standard Test Method for Measurement of Fracture Toughness, American Society for Testing and Materials, Philadelphia, USA

[4] Joyce, J.A., Hackett, E.M. and Roe, C.(1993), "Effects of Crack Depth and Mode of Loading on the J-R Curve Behavior of a High-Strength Steel", Constraint Effects in Fracture, Hackett, E.M., Schwalbe, K.-H., and Dodds, R.H. Jr., eds, ASTM STP 1171, Philadelphia, pp. 239-263.

[5] ESIS P2-92 (1992) ESIS Procedure for Determining the Fracture Behavior of Materials, European Structural Integrity Society, Delft, The Netherlands.

[6] N. P. O'Dowd and C. F. Shih, , Family of crack-tip fields characterized by a triaxiality parameter – I. Structure of fields, *J. Mech. Phys. Solids*, vol. 39, pp 989-1015, 1991

[7] Betegon, C. and Hancock, J.W., Two-Parameter Characterization of Elastic-Plastic Crack Tip Fields, *Journal of Applied Mechanics*, Vol.58, pp. 104-116, 1991

[8] Al-Ani, A.M. and Hancock, J.W., J-Dominance of Short Cracks in Tension and Bending, *Journal of Mechanics and Physics of Solids*, Vol. 39, pp. 23-43, 1991

[9] O'Dowd, N.P. and Shih, C. F., Family of Crack-Tip Fields Characterized by a Triaxiality Parameter-II. Fracture Application, *Journal of Mechanics and Physics of Solids*, Vol. 39, pp. 939-963, 1991

[10] Shen, G., Tyson, W. R. and Glover, A. G., Effect of Constraint on Fracture Toughness of Linepipe Steel, Modeling and Simulation Based Engineering, eds., Atluri, S. N. and O'Donoghue, P. E., vol. II, pp. 1347-1352, 1998

[11] Ainsworth, A., A Constraint-based Failure Assessment Diagram for Fracture Assessment, *Int. J. Press. Vessels & Piping*, vol.64, pp. 277-285, 1995

[12] Dodds, R. H. Jr., Anderson, T. L. and Kirk, M. T. , A Framework to Correlate a/W Ratio Effects on Elastic-Plastic Fracture Toughness (J_c), *International Journal of Fracture*, 48, pp.1-22, 1991.

[13] Shih, C. F., Brown University Report, MRL E149, 1983.

P517271.PDF [Page: 29 of 59]

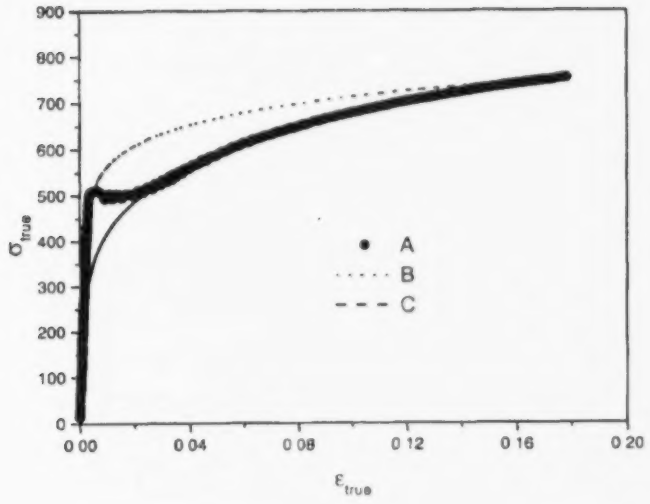

Fig. 1 True stress/true strain curve (A) and Ramberg-Osgood curve fits (B, C)

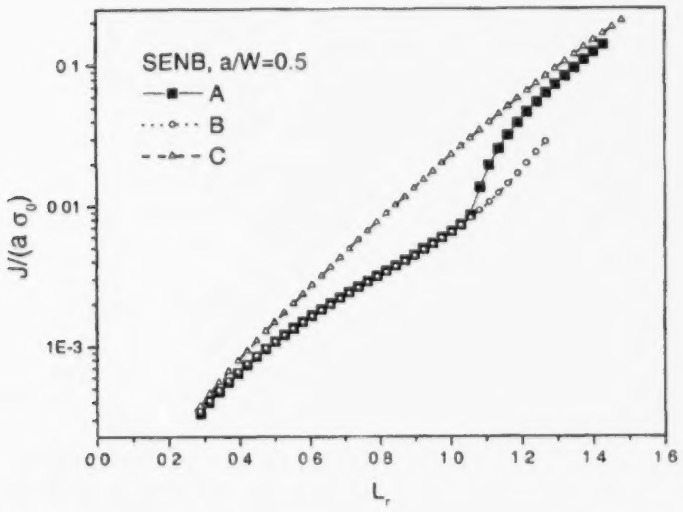

Fig. 2 Normalized J-integral as a function of L_r

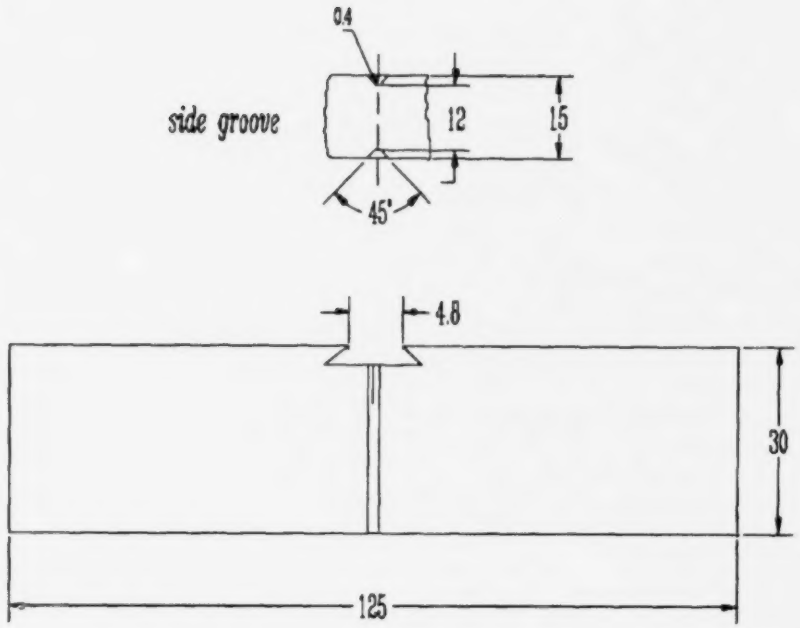

Fig. 3 Specimen geometry (mm)

P517271.PDF [Page: 31 of 59]

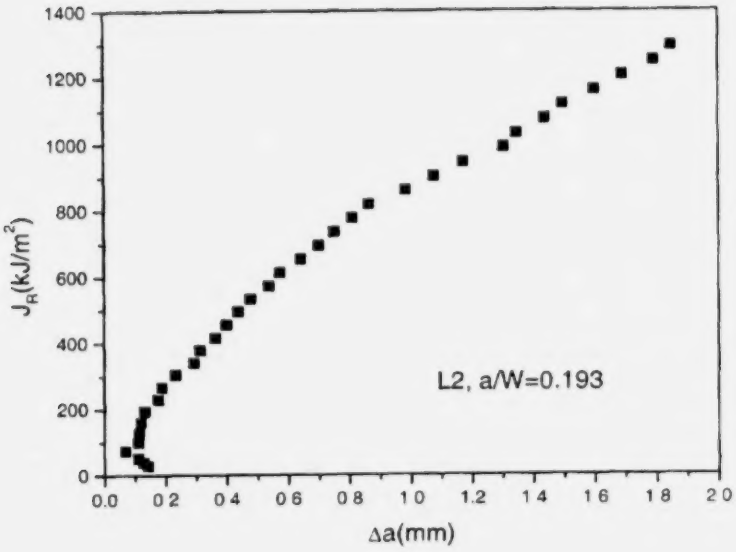

Fig. 4a J-resistance curve for Sample L2

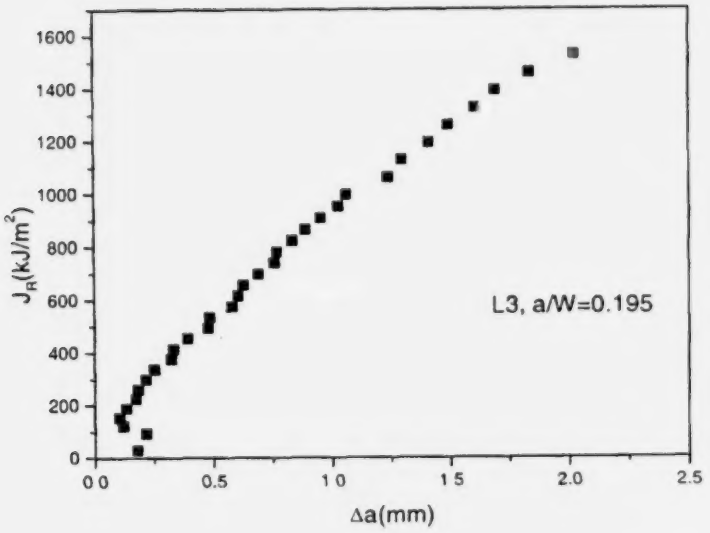

Fig. 4b J-resistance curve for Sample L3

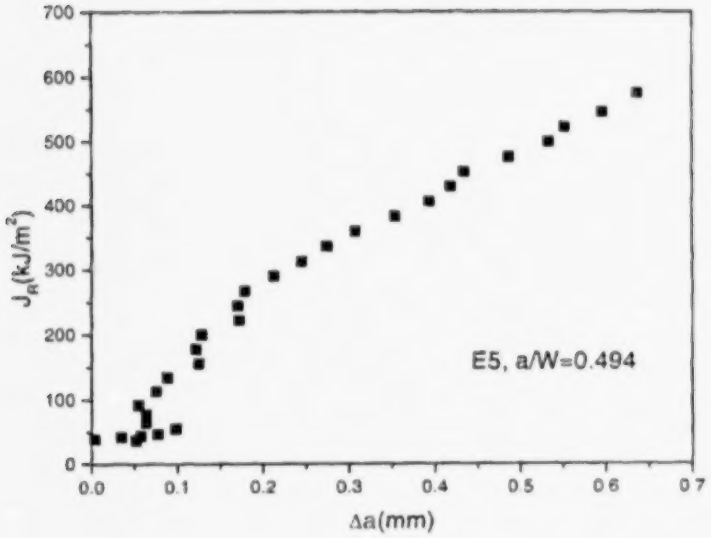

Fig. 4c J-resistance curve for Sample E5

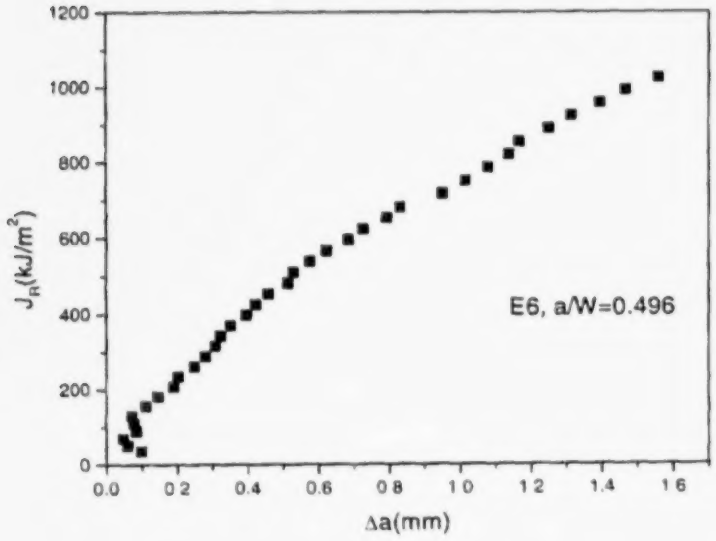

Fig. 4d J-resistance curve for Sample E6

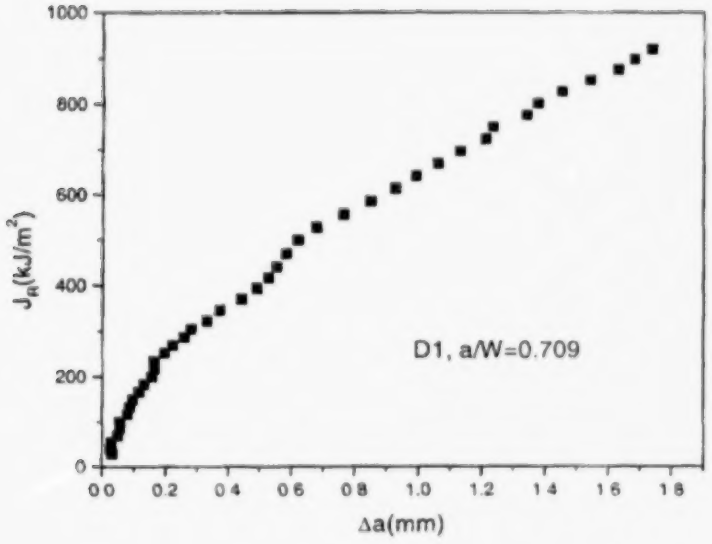

Fig. 4e J-resistance curve for Sample D1

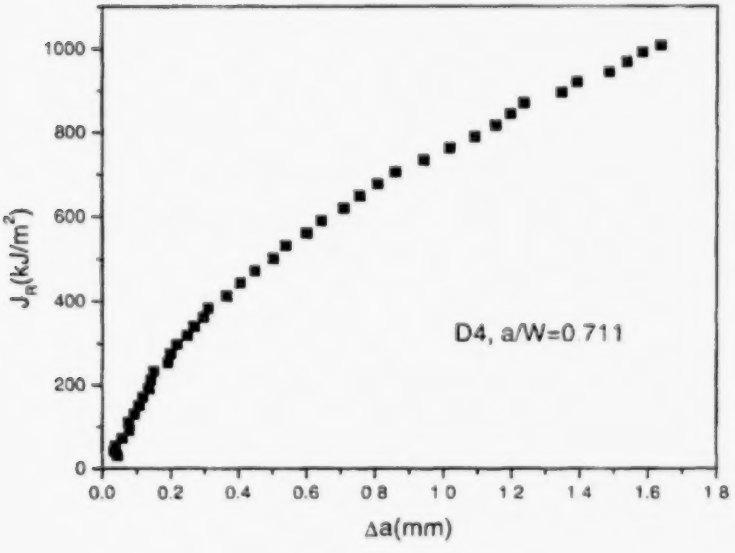

Fig. 4f J-resistance curve for Sample D4

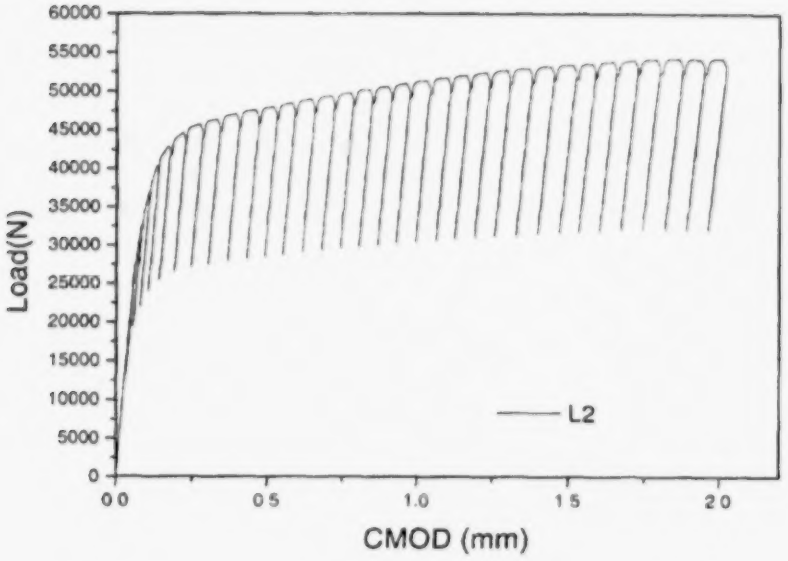

Fig. 6a Load vs. crack mouth opening displacement for Sample L2

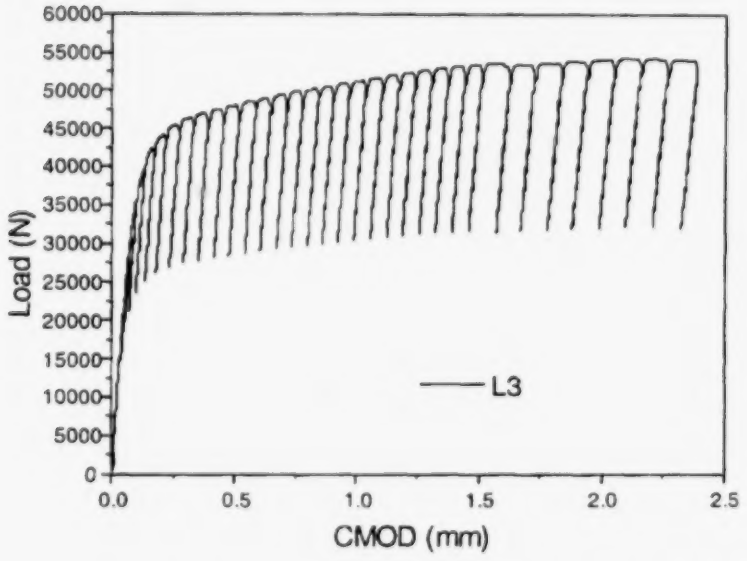

Fig. 6b Load vs. crack mouth opening displacement for Sample L3

PS17271.PDF [Page: 35 of 59]

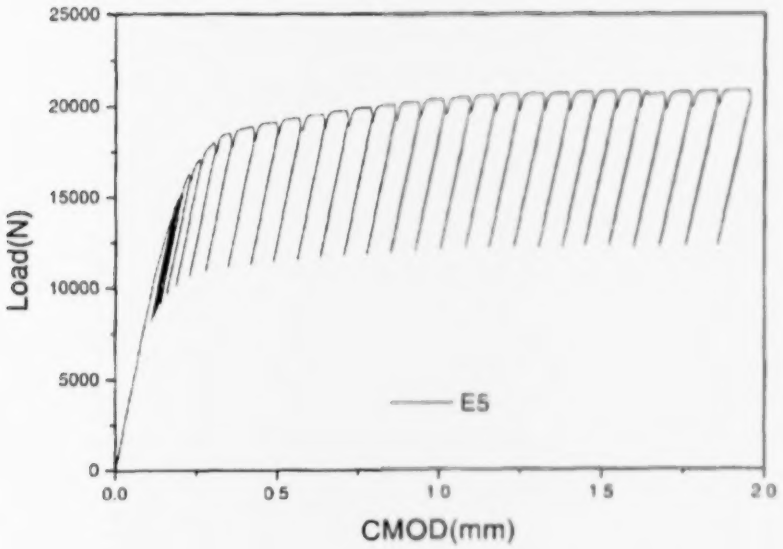

Fig. 5c Load vs. crack mouth opening displacement for Sample E5

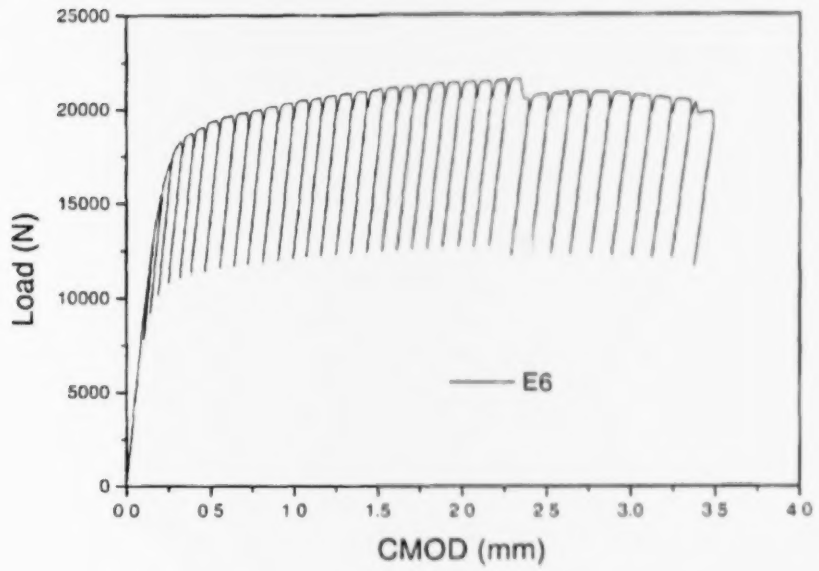

Fig. 5d Load vs. crack mouth opening displacement for Sample E6

P517271.PDF [Page: 36 of 59]

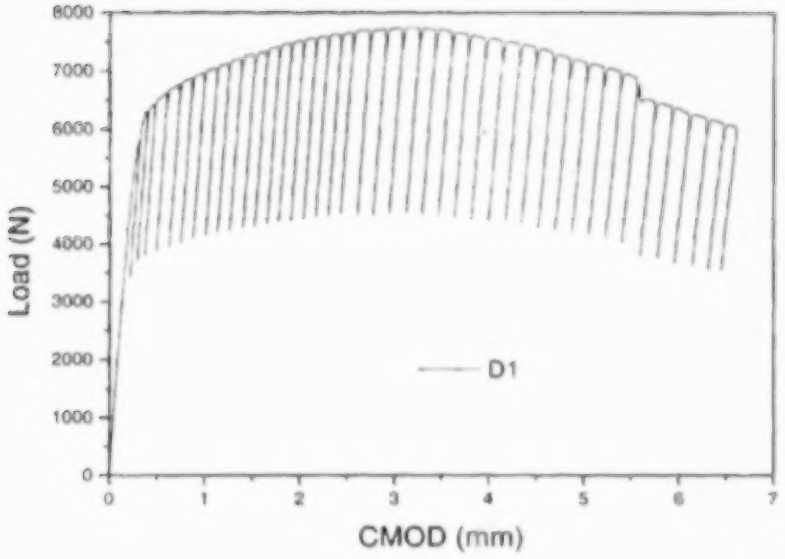

Fig. 5e Load vs. crack mouth opening displacement for Sample D1

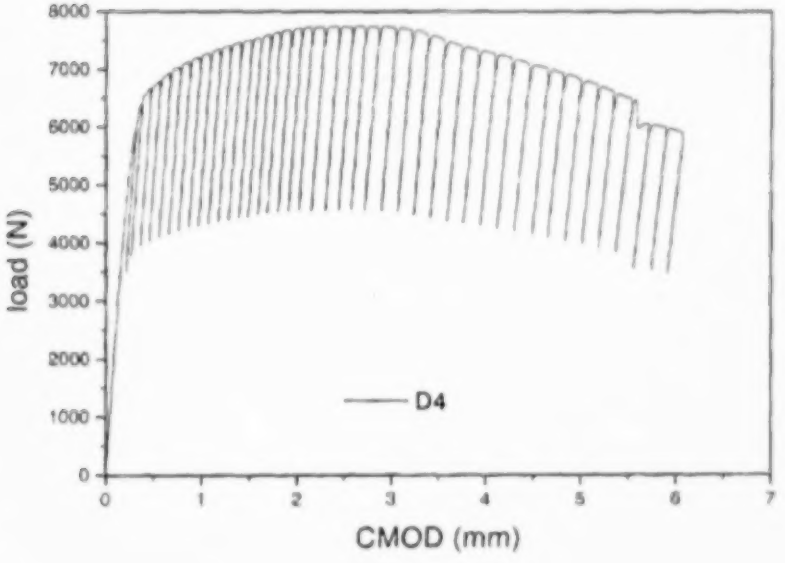

Fig. 5f Load vs. crack mouth opening displacement for Sample D4

P517271.PDF [Page: 37 of 58]

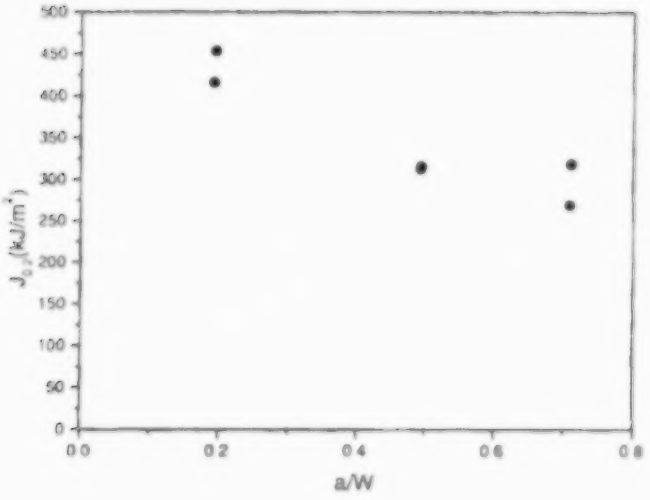

Fig. 6 J-resistance ($J_{0.2}$) as a function of a/W ($J_{0.2}$ is the J-resistance at 0.2 mm crack extension measured directly by compliance unloading; the crack length was not revised by using ASTM E1820)

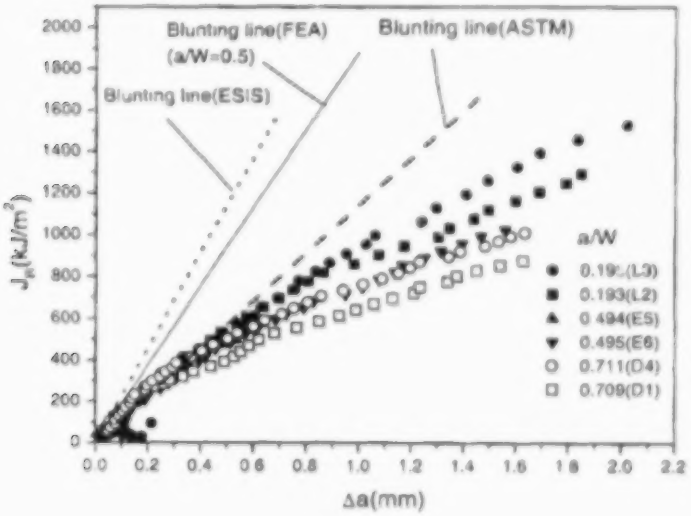

Fig. 7 J-resistance curves for SENB samples(the initial crack lengths have been revised by using eqn (A11.1) in ASTM E1820)

P517271.PDF [Page: 38 of 59]

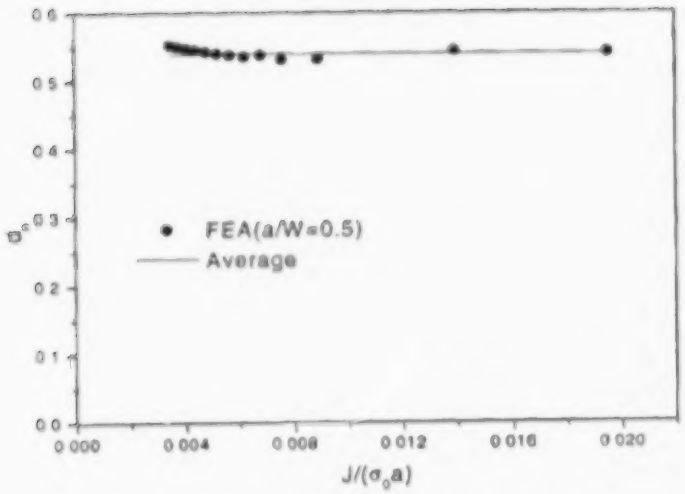

Fig. 8 d_n as a function of normalized J-integral, calculated for actual σ-ε data

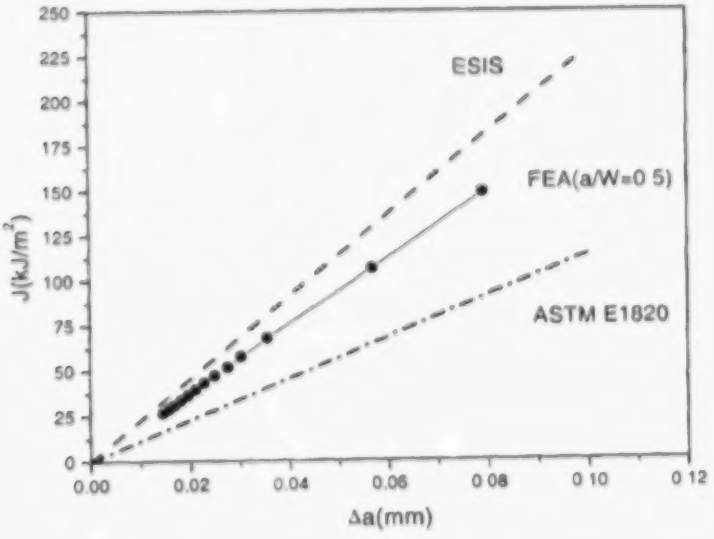

Fig. 9 Blunting line for SENB geometry (a/W=0.5);

P517271.PDF [Page: 39 of 59]

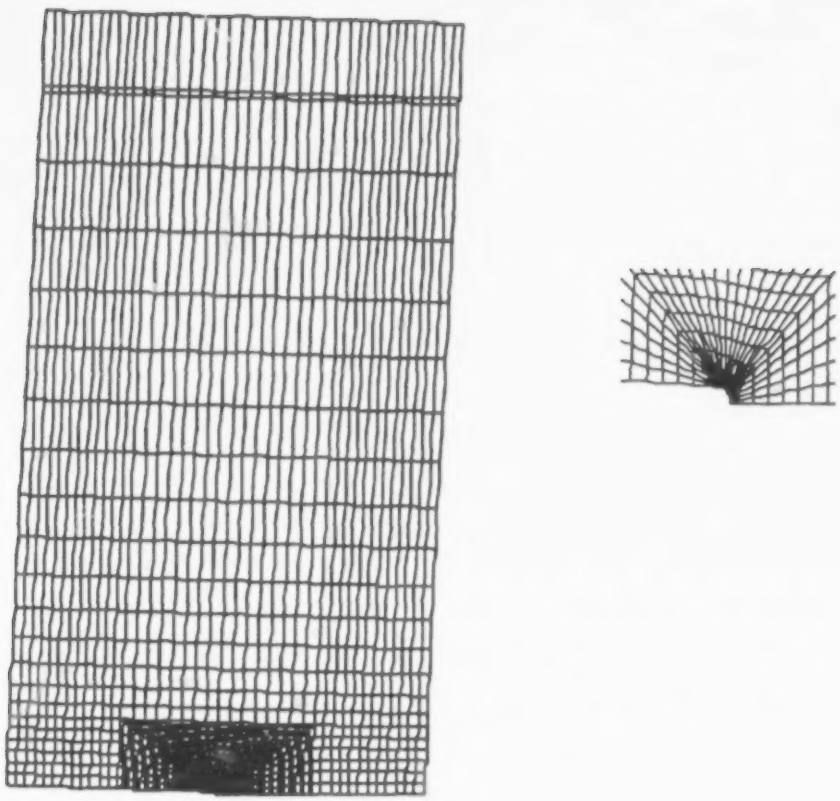

Fig. 10 Finite element mesh for a SENB sample and its deformed crack tip

P517271.PDF [Page: 40 of 59]

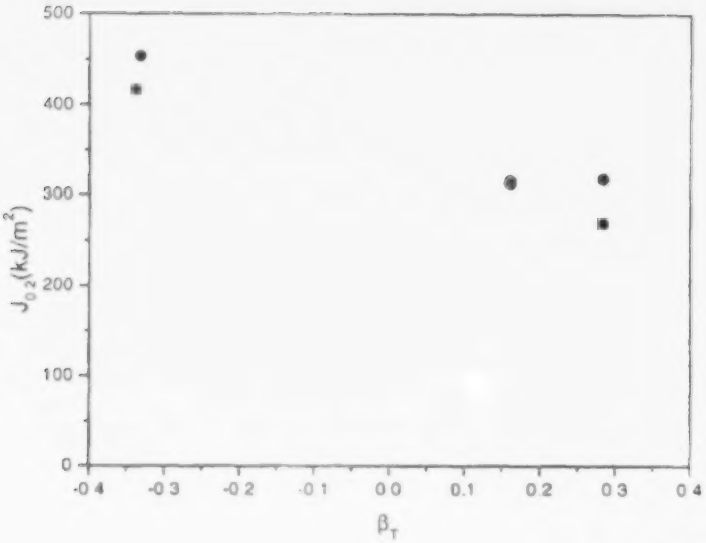

Fig. 11 $J_{0.2}$ vs β_T for SENB samples with different a/W

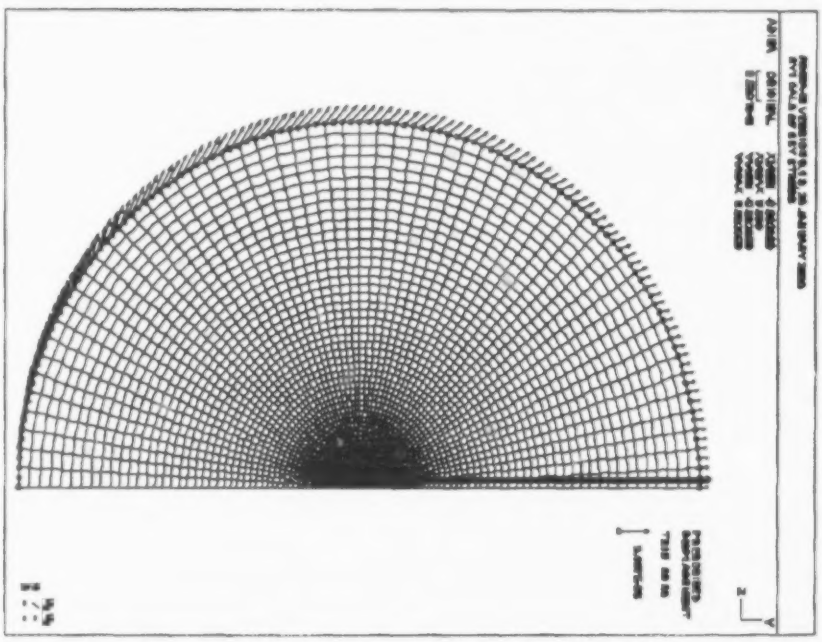

Fig. 12 Finite element mesh for boundary layer method

P517271.PDF [Page 41 of 59]

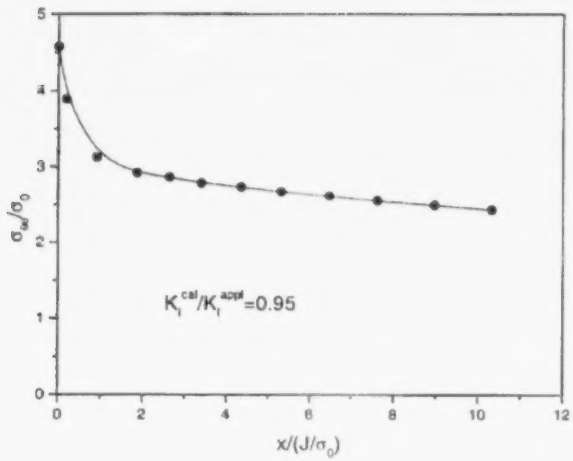

Fig. 13 Normalized opening stress at crack tip under plane strain small-scale yielding (SYY)

P517271.PDF [Page: 42 of 59]

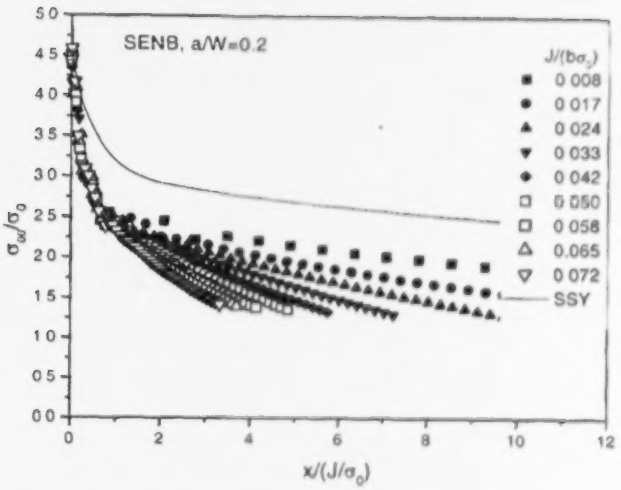

Fig. 14 Normalized crack opening stress as a function of normalized distance from crack tip, a/W=0.2

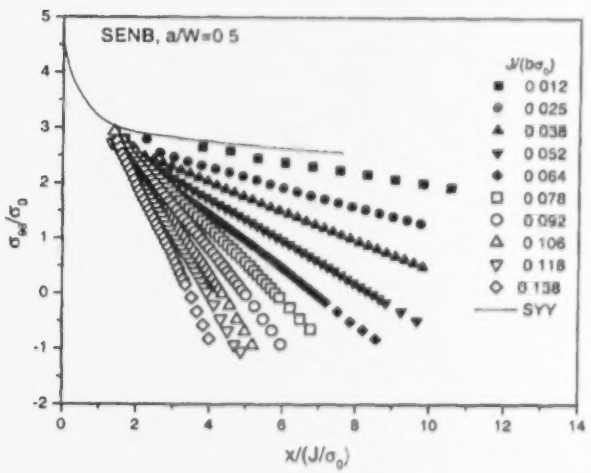

Fig. 15 Normalized crack opening stress as a function of normalized distance from crack tip, a/W=0.5

P517271.PDF [Page: 43 of 59]

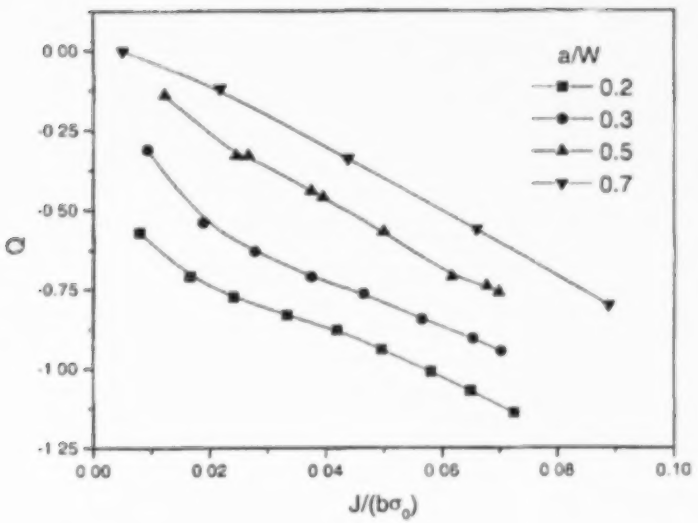

g. 16 Q as a function of applied driving force for SENB geometry

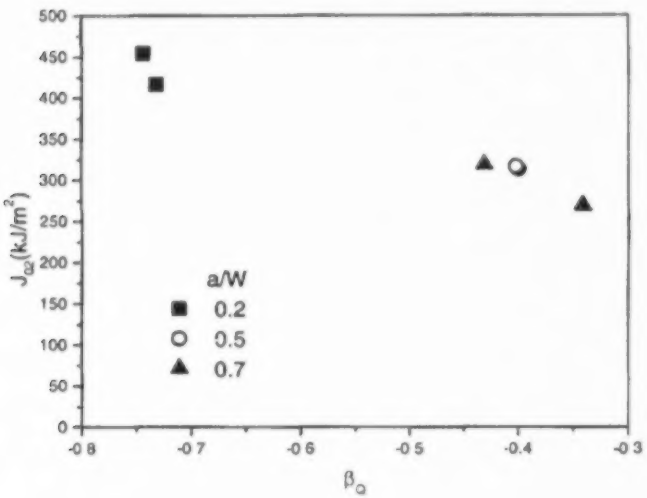

Fig. 17 $J_{0\,2}$ as a function of β_Q for SENB samples

APPENDIX A

Notes on macro-fracture surface and stretch zone width measurements

Notes on macro-fracture surface and stretch zone width measurements

Fig. A1 shows an optical macrograph of fracture surfaces of three samples, L2, E6, and D1, with a/W approximately 0.2, 0.5 and 0.7 respectively. Splitting is evident at the centre of sample E6. Fig. A2 shows the fatigue precracked regions, stretch zones and ductile tearing regions in the three samples near the mid-thickness. Crack extension occurred by ductile tearing in all three samples. The tearing regions show a wide range of dimple sizes (Fig. A3).

The stretch zone (SZ) observed on the fracture surfaces corresponds to the blunting of the initially sharp crack during loading. The stretch zone width (SZW) is half the crack tip opening displacement (CTOD). Therefore, the critical SZW has been related to fracture toughness properties (J_{Ic} or Critical CTOD) in European Structural Integrity Society (ESIS) and in Japan Society of Mechanical Engineers (JSME) elastic-plastic fracture toughness standards [A1, A2].

The SZW was measured following the ESIS procedure [A1], except that five measurement positions were used instead of nine. SEM fractographs were taken along the specimen thickness at five equally spaced positions. Five SZW measurements were made on each fractograph (Fig. A4) and the average of these measurements was recorded for each position. The measurements were done carefully so that no dimple (i.e. no part of the tearing region) was included in any stretch zone. The difficulties in accurately measuring the SZW have been discussed at length by Schwalbe et al. [A3]. The procedure used here yields conservative SZW values. The average at each of the five measurement positions and the overall average for each sample are reported in Table A1.

Table A1 Stretch zone width values (mm)

Sample	Measurement position					
	1	2	3	4	5	Average
L2	0.019	0.014	0.014	0.027	0.014	0.017
E6	0.012	0.025	0.028	0.031	0.014	0.022
D1	0.023	0.029	0.012	0.031	0.012	0.022

Further SZW measurements were made on the opposite fracture surface of sample E6 following the same procedure. The average values at the five measurement positions were 0.024, 0.040, 0.040, 0.047 and 0.031 mm, yielding an overall average of 0.037 mm. This value is in only modest agreement with the value of 0.022 mm measured on the other fracture surface (Table A1). The SWZs in two mating fracture surfaces may not always be

the same because the crack may not start at a symmetrical point of the blunting region, although Schwalbe [A3] has reported measurements that supported symmetrical blunting and initiation.

The values in Table A1 are surprisingly small, even given the conservative nature of the definition used. This definition requires that no dimple (i.e. no part of the tearing region) be included in the stretch zone. With this definition, some regions that appear to contain features more characteristic of stretching rather than tearing are excluded from the SZ. If some small voids or secondary cracks in the stretch zones are ignored, then significantly larger stretch zones result; and these may be more realistic. Also, as is well known, the dividing line between the SZ and the tearing region is often not clearly defined and hence the SZW measurement is subjective. To test this, the SZWs of the steel based on fractographs taken near the middle part of the samples (Fig. A2), considered to be the most appropriate location for measuring SZW [A4, A5], were measured by three different researchers experienced in fracture mechanics. The measurements by different persons were found to typically differ from the average by 25%; as reported in Table A2, the SZW values range from 0.035-0.082 mm for sample L2, 0.049-0.074 mm for sample E6 and 0.075-0.139 mm for sample D1. The SZW is difficult to determine because of the non-uniformity of the SZW along the crack front and the existence of voids or secondary cracks inside the stretch zone. Other factors include intrinsic variability and subjective judgments [A5, A6].

Table A2 Stretch zone width values (mm) based on fractographs in Fig. A2

Sample	SZW (mm)			
	Researcher 1	Researcher 2	Researcher 3	Average
L2	0.066	0.035	0.082	0.061
E6	0.068	0.049	0.074	0.064
D1	0.097	0.075	0.139	0.104

Although it was expected that SZW values would be larger for smaller a/W since shallower cracks are associated with less constraint and higher toughness, this was not reflected in the measurements. The significance of the relative constancy of SZW with crack depth is surprising, and is not understood.

The initiation J values were determined by applying procedures according to ASTM E813, ASTM E1820, and from SZWs using the blunting line equation and are listed in Table A3. Also listed in Table A3 are the values of J at 0.2 mm total crack growth, $J_{0.2}$, reported above.

Table A3 J_Q values estimated from ASTM E 1820 and E 813, and from SZW

Procedure	J_Q (kJ/m^2)		
	L2	E6	D1
ASTM E 813 (intersection value, with M=2)	646	464	411
ASTM E 1820 (0.2 mm offset value, with M=2)	842	636	525
(0.2 mm offset value with M=3.3)	600	463	356
From avg. SZW in Table A1	38	50	50
From avg. SZW in Table A2	139	146	237
At 0.2 mm crack growth ($J_{0.2}$)	417	316	269

The original ASTM E813-81 procedure [A7] uses an intersection method, i.e. J_Q is defined as the intersection of a linear regression line of the J-R curve with the ASTM blunting line with M=2. E813 was discontinued in 1997 as it was superseded by E1820. E1820 employs an offset method with the slope of the blunting and offset lines calculated using either M=2 or M evaluated experimentally. In the present work, a value of 3.3 was used for M since this value is consistent both with experimental results and with the FEM calculations reported above. The resistance curve for sample E6 and the analysis according to E1820 are shown in Fig. A5.

The J_Q values determined from the E813-81 procedure are significantly lower than those from E1820 with M=2 but are close to those with M=3.3. The J_Q values determined according to E1820 are much larger than those determined using the SZW measurements. Recent studies [A8, A9] also showed a similar trend, i.e. the critical J values by the ASTM procedure with M = 2 were higher than the values determined at physical crack initiation using the SZWs. $J_{0.2}$ values at 0.2 mm crack growth are, of course, smaller than the offset values of ASTM E1820; the latter necessarily define a point on the resistance curve that includes 0.2 mm blunting plus an indeterminate amount of tearing.

Most J_Q values determined according to the E1820 and original E813 procedures did not meet the size requirement for J_{Ic} in E1820, except for the 0.2 mm offset value with M=3.3 for sample D1. The J_Q values from SZW measurement met the size requirement in E1820. As shown in Fig. A5 for sample E6, J_{max} (minimum of $b\sigma_Y/20$ and $B\sigma_Y/20$) and Δa_{max} ($0.25b_0$) refer to the "measurement capacity"of the sample; the valid part of the resistance curve is that lying within the rectangle bounded by J_{max} and Δa_{max} . The values of J_{lim} ($b_0\sigma_Y/15$) and Δa_{lim} (defined by the intersection of the resistance curve with the 1.5mm exclusion line), together with an exclusion line drawn 0.15 mm from the construction line, are used in selecting data points for fitting the power-law line used in evaluating J_Q by the

offset method. The 0.2mm offset line is shown in Fig. A5. Two regression lines are shown in Fig. A5: one according to the equation given in E 1820, and the other a single-term power law of the form $J=J_0(\Delta a)^m$ with J_0 =775 kJ/m^2 and m=0.68 shown for comparison. The single-term fit is at least as acceptable as the E1820 form.

References

[A1] ESIS Procedure for Determining the Fracture Behaviour of Materials, ESIS P2-92, European Structural Integrity Society, Delft, the Netherlands, January 1992.

[A2] Standard Method of Test for Elastic-Plastic Fracture Toughness J_{Ic}, Japan Society of Mechanical Engineers, JSME S 001-81, 1981.

[A3] K.-H. Schwalbe, B. Hayes, K. Baustian, A. Cornec, R. Gordon, M. Homayun and B. Voss, "Validation of the fracture mechanics test method P1-87D (ESIS P1-90/ESIS P1-92), Fatigue Frac. Engng. Mater. Struc., Vol. 16, 1993, pp. 1231-1284.

[A4] H. Kobayashi, H. Nakamura and H. Nakazawa, " Evaluation of Blunting Line and Elastic-Plastic Fracture Toughness", Elastic-Plastic Fracture: Vol. II-Fracture Resistance Curves and Engineering Applications, ASTM STP 803, C.F. Shih and J.P.. Gudas, Eds., ASTM, 1983, pp. II-420-II-438.

[A5] C.V. Hyatt and J.R. Matthews, "Variation of Stretch Zone Width with J, Loading Rates, Temperature and Pre-Crack Depth", Int. J. Fracture, Vol. 66, 1994, pp. 19-32.

[A6] J. Smith, M.N. Bassim and C.D. Liu, "Effects of Fatigue Precracking on Stretch Zone Formation", Engng. Fract. Mech., Vol. 52, No. 3, 1995, pp. 401-408.

[A7] "Standard Test for J_{Ic}, A Measure of Fracture Toughness", E 813-81, Annual Book of ASTM Standards, ASTM, Philadelphia, 1981.

[A8] P. Deimel, H. Fischer and M. Hoffmann, "Strength and Toughness Properties of Two Nitrogen Alloyed Stainless Steels and Their Submerged Arc Weldments at Cryogenic Temperatures", J Mater. Sci., Vol. 33, 1998, pp. 1105-1116.

[A9] H.W. Viehrig, J. Boehmert, H. Richter and M. Valo, "Use of Instrumented Charpy Test for Determination of Crack Initiation Toughness", Pendulum Impact Testing: A Century of Progress, STP 1380, T A. Siewert and M.P. Manahan, Sr., Eds., ASTM, West Conshohocken, PA, 2000, pp. 355-365.

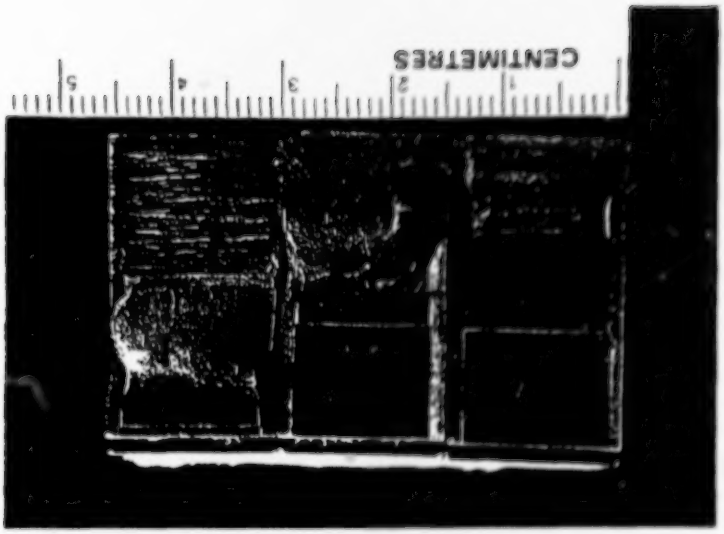

Fig. A1 Optical macrograph of fracture surfaces of 3 fracture toughness samples. Left to right L2, E6, and D1 with a/W nominally 0.2, 0.5 and 0.7 respectively.

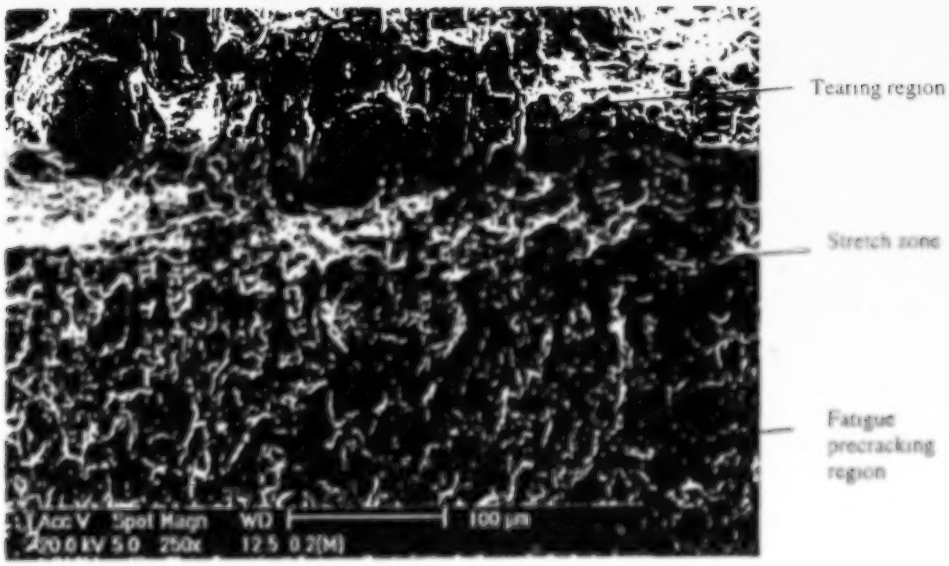

(a) sample L2 (a/W=0.2)

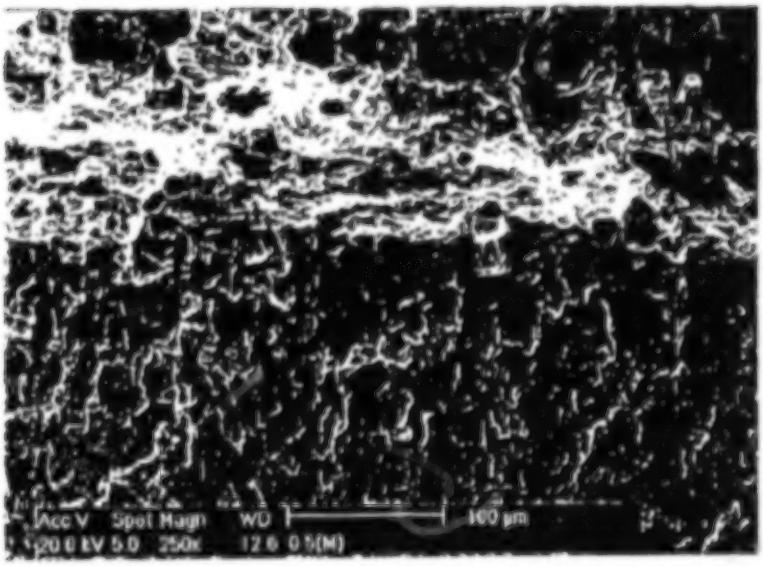

(b) sample E6 (a/W=0.5)

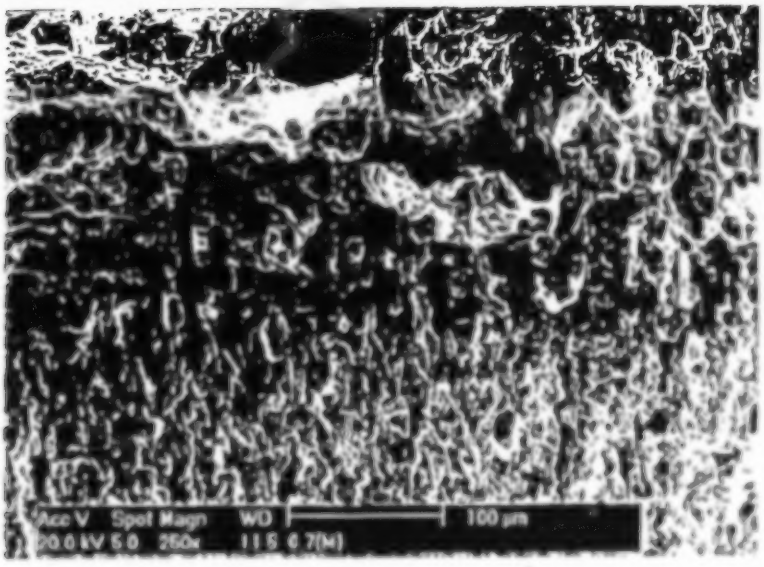

(c) sample D1 (a/W ~0.7)

Fig. A2 SEM fractograph of fatigue precracked region, stretch zone and tearing region near the middle part of the three samples

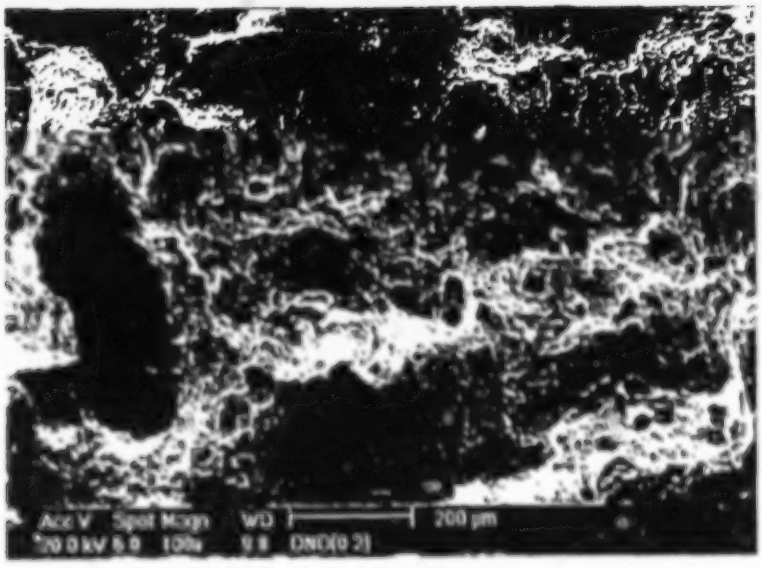

Fig. A3 SEM fractograph of the ductile region of sample L2

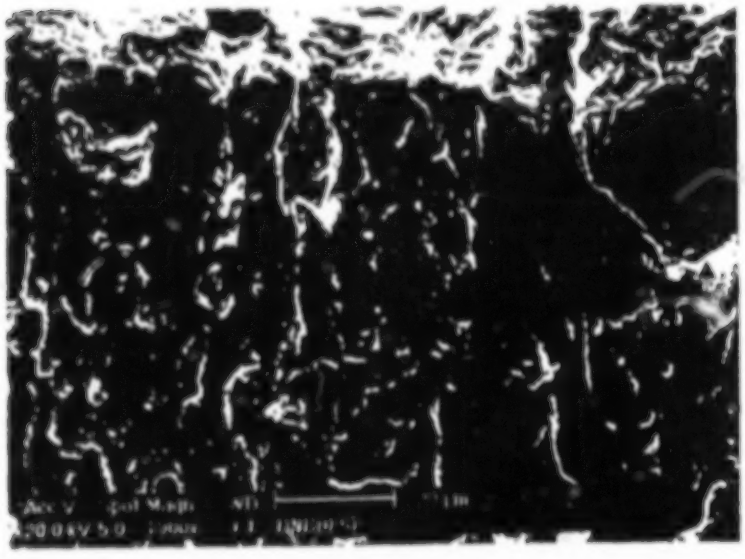

Fig. A4 Stretch zone of sample E6 in the mid-thickness position (measurement position 3)

9517271.PDF [Page: 53 of 59]

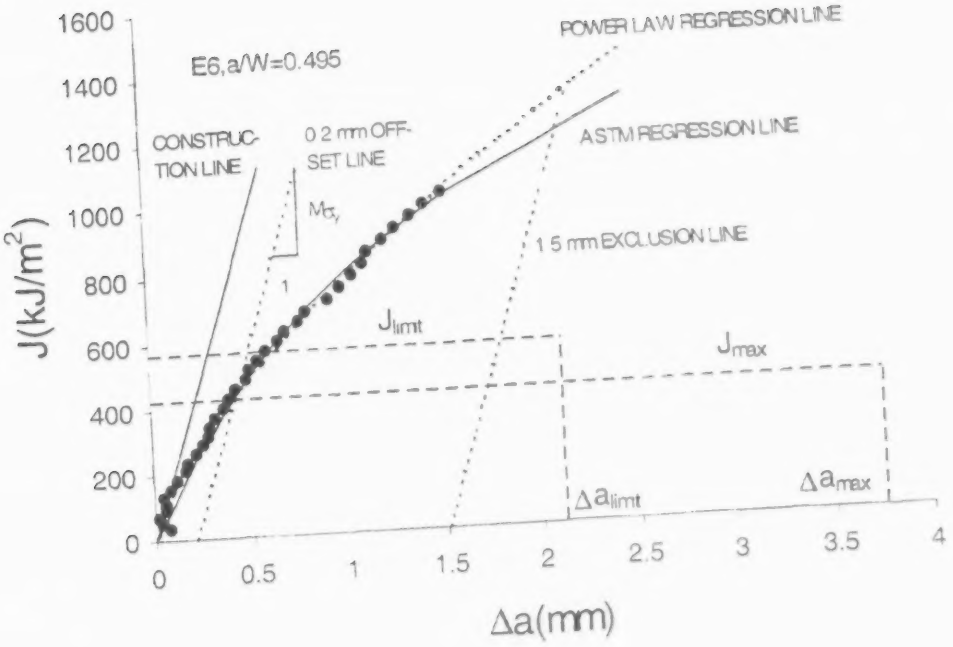

Fig. A5 Resistance curve for sample E6 analysed according to ASTM E1820

P517271.PDF [Page: 54 of 59]

List of figures

Figure 1. True Stress/true strain curve (A) and Ramberg-Osgood curve fits (B,C) 18

Figure 2. Normalized J-integral as a function of L_r 18

Figure 3. Specimen geometry (mm) 19

Figure 4a. J-resistance curve for Sample L2 20

Figure 4b. J-resistance curve for Sample L3 20

Figure 4c. J-resistance curve for Sample E5 21

Figure 4d. J-resistance curve for Sample E6 21

Figure 4e. J-resistance curve for Sample D1 22

Figure 4f. J-resistance curve for Sample D4 22

Figure 6a. Load vs. crack mouth opening displacement for Sample L2 23

Figure 6b. Load vs. crack mouth opening displacement for Sample L3 23

Figure 5c. Load vs. crack mouth opening displacement for Sample E3 24

Figure 5d. Load vs. crack mouth opening displacement for Sample E6 24

Figure 5e. Load vs. crack mouth opening displacement for Sample D1 25

Figure 5f. Load vs. crack mouth opening displacement for Sample D4 25

P517271.PDF [Page: 55 of 59]

Figure 6. J-resistance ($J_{0.2}$) as a function of a/W ($J_{0.2}$ is the J-resistance 26
at 0.2 mm crack extension measuremend directly by compliance unloading; the
crack length was not revised by using ASTM E1820)

Figure 7. J-resistance curves for SENB samples (the initial crack lengths 26
have been revised by suing eqn (A11.1) in ASTM E1820)

Figure 8. d_n as a function of normalized J-integral, calculated for actural σ ε data 27

Figure 9. Blunting line for SENB geometry (a/W=0.5); 27

Figure 10. Finite element mesh for a SENB sample and its deformed crack tip 28

Figure 11. $J_{0.2}$ vs β_T for SENB samples with different a/W 29

Figure 12. Finite element mesh for boundary layer method 29

Figure 13. Normalized opening stress at crack tip under plan strain small-scale 30
yielding (SYY)

Figure 14. Normalized crack opening stress as a function of 31
normalized distance from crack tip, a/W=0.2

Figure 15. Normalized crack opening stress as a function of 31
normalized distance from crack tip, a/W=0.5

Figure 16. Q as a function of applied driving force for SENB geometry 32

Figure 17. $J_{0.2}$ as a function of β_Q for SENB samples 32

Annexes

Annex A Notes on macro-fracture surface and stretch zone width measurements

UNCLASSIFIED
SECURITY CLASSIFICATION OF FORM
(highest classification of Title, Abstract, Keywords)

DOCUMENT CONTROL DATA

(Security classification of title, body of abstract and indexing annotation must be entered when the overall document is classified)

1 ORIGINATOR (the name and address of the organization preparing the document Organizations for whom the document was prepared, e g Establishment sponsoring a contractor's report, or tasking agency, are entered in section 8)

Materials Technology Laboratory, CANMET
568 Booth Street, Ottawa, Ontario, Canada, K1A0G1

2 SECURITY CLASSIFICATION (overall security classification of the document including special warning terms if applicable)

UNCLASSIFIED

3 TITLE (the complete document title as indicated on the title page Its classification should be indicated by the appropriate abbreviation (S,C,R or U) in parentheses after the title)

Constraint Effects on Fracture Toughness

4 AUTHORS (Last name, first name, middle initial If military, show rank, e g Doe, Maj John E)

G. Shen, S. Xu, and W.R. Tyson

5 DATE OF PUBLICATION (month and year of publication of document)	6a NO OF PAGES (total containing information Include Annexes, Appendices, etc)	6b NO OF REFS (total cited in document)
July 2001	42	22

7 DESCRIPTIVE NOTES (the category of the document, e g technical report, technical note or memorandum If appropriate, enter the type of report, e g interim, progress, summary, annual or final Give the inclusive dates when a specific reporting period is covered)

CONTRACTOR REPORT

8 SPONSORING ACTIVITY (the name of the department project office or laboratory sponsoring the research and development Include address)

Defence Research Establishment Atlantic
PO Box 1012, Dartmouth, NS, Canada B2Y 3Z7

9a PROJECT OR GRANT NO (if appropriate, the applicable research and development project or grant number under which the document was written Please specify whether project or grant)	9b CONTRACT NO (if appropriate, the applicable number under which the document was written)

10a ORIGINATOR'S DOCUMENT NUMBER (the official document number by which the document is identified by the originating activity This number must be unique to this document)	10b OTHER DOCUMENT NOs (Any other numbers which may be assigned this document either by the originator or by the sponsor)
	DREA CR 2001-91

11 DOCUMENT AVAILABILITY (any limitations on further dissemination of the document, other than those imposed by security classification)

(X) Unlimited distribution
( ) Defence departments and defence contractors; further distribution only as approved
( ) Defence departments and Canadian defence contractors; further distribution only as approved
( ) Government departments and agencies; further distribution only as approved
( ) Defence departments; further distribution only as approved
( ) Other (please specify):

12 DOCUMENT ANNOUNCEMENT (any limitation to the bibliographic announcement of this document This will normally correspond to the Document Availability (11) However, where further distribution (beyond the audience specified in (11) is possible, a wider announcement audience may be selected)

UNCLASSIFIED
SECURITY CLASSIFICATION OF FORM

UNCLASSIFIED
SECURITY CLASSIFICATION OF FORM
(highest classification of Title, Abstract, Keywords)

13. ABSTRACT (a brief and factual summary of the document It may also appear elsewhere in the body of the document itself It is highly desirable that the abstract of classified documents be unclassified Each paragraph of the abstract shall begin with an indication of the security classification of the information in the paragraph (unless the document itself is unclassified) represented as (S), (C), (R), or (U) It is not necessary to include here abstracts in both official languages unless the text is bilingual)

Fracture resistance curves have been measured for a CSA 350WT ship plate using different a/W ratios, and stretch-zone-width (SZW) measurements have been made on the fracture surfaces. Associated calculations using finite element analysis (FEA) have also been performed, with special attention paid to the crack tip blunting behaviour.

It has been confirmed that the fracture resistance increases with decreasing constraint, i.e. with decreasing a/W. It has also been shown that the blunting line slope $M\sigma_y$ depends on constraint as well as on material properties. FEA results indicate that M lies between the value recommended in ASTM standards (M=2) and that suggested by the European Structural Integrity Society (ESIS) (M=4 for this material), being closer to the ESIS value.

The subjective nature of the measurement made it difficult to derive reproducible SZW values, and a recently developed ESIS procedure produced very conservative results. It is difficult to clearly distinguish between the stretch zone and the tearing regions, particularly when the resistance curve data is described using a power-law equation. This suggests that it would be preferable to define toughness by means of a value of J or CTOD at a specific amount of crack growth, e.g. 0.2 mm, without distinguishing between blunting and tearing contributions.

14. KEYWORDS, DESCRIPTORS or IDENTIFIERS (technically meaningful terms or short phrases that characterize a document and could be helpful in cataloguing the document They should be selected so that no security classification is required Identifiers, such as equipment model designation, trade name, military project code name, geographic location may also be included If possible keywords should be selected from a published thesaurus e g Thesaurus of Engineering and Scientific Terms (TEST) and that thesaurus-identified If it not possible to select indexing terms which are Unclassified, the classification of each should be indicated as with the title)

fracture toughness
constraint
crack blunting
stretch zone
finite element analysis

UNCLASSIFIED
SECURITY CLASSIFICATION OF FORM